WSRC-TR-2001-00245, REV. 0

Key Words:
XAFS, MST
Strontium

Retention:
Permanent

Characterization of Sorbed Strontium on Monosodium Titanate

Martine C. Duff, Douglas B. Hunter, David T. Hobbs and Samuel D. Fink

REPORT DATE: JUNE 25, 2001

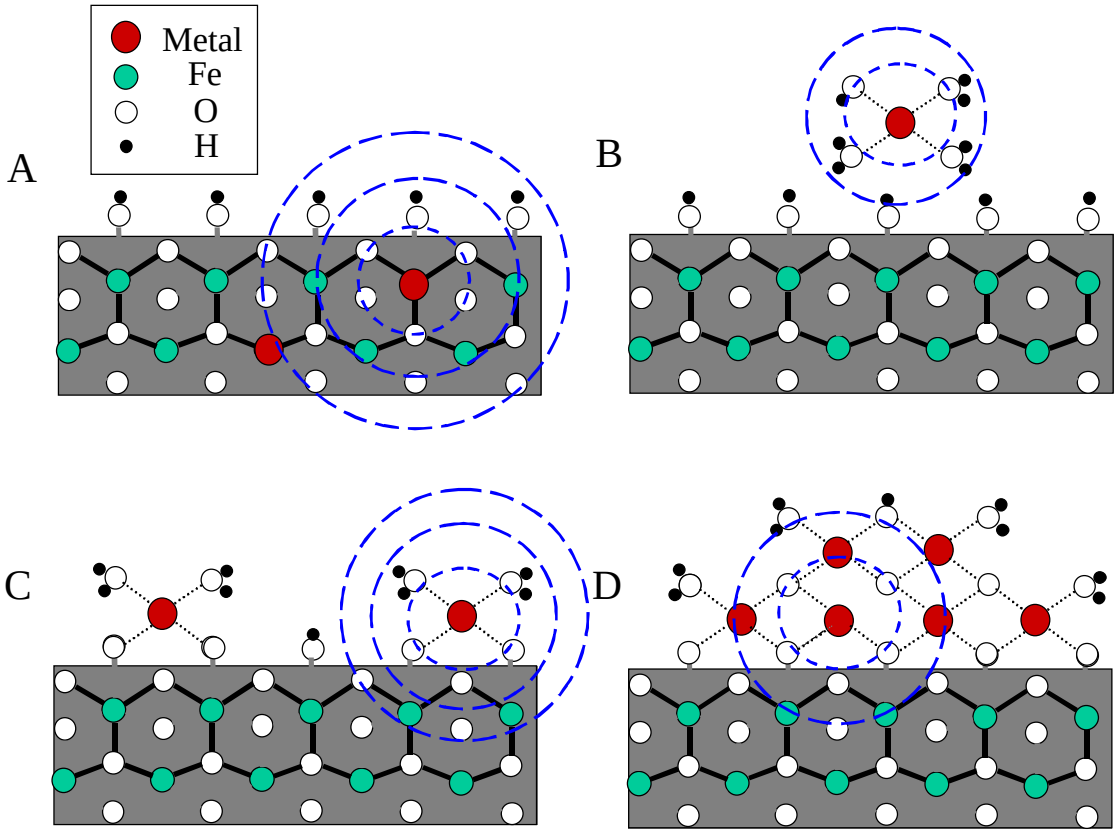

Westinghouse
Savannah River Company
Aiken, SC 29808

Prepared for the U.S. Department of Energy
under Contract Number DE-AC09-96SR18500

This document was prepared in conjunction with work accomplished under Contract No. DE-AC09-96SR18500 with the U.S. Department of Energy.

DISCLAIMER

This report was prepared as an account of work sponsored by an agency of the United States Government. Neither the United States Government nor any agency thereof, nor any of their employees, makes any warranty, express or implied, or assumes any legal liability or responsibility for the accuracy, completeness, or usefulness of any information, apparatus, product or process disclosed, or represents that its use would not infringe privately owned rights. Reference herein to any specific commercial product, process or service by trade name, trademark, manufacturer, or otherwise does not necessarily constitute or imply its endorsement, recommendation, or favoring by the United States Government or any agency thereof. The views and opinions of authors expressed herein do not necessarily state or reflect those of the United States Government or any agency thereof.

This report has been reproduced directly from the best available copy.

Available for sale to the public, in paper, from: U.S. Department of Commerce, National Technical Information Service, 5285 Port Royal Road, Springfield, VA 22161, phone: (800) 553-6847, fax: (703) 605-6900, email: orders@ntis.fedworld.gov online ordering: http://www.ntis.gov/ordering.htm

Available electronically at http://www.doe.gov/bridge

Available for a processing fee to U.S. Department of Energy and its contractors, in paper, from: U.S. Department of Energy, Office of Scientific and Technical Information, P.O. Box 62, Oak Ridge, TN 37831-0062, phone: (865) 576-8401, fax: (865) 576-5728, email: reports@adonis.osti.gov

Key Words:
XAFS, MST
Strontium

Retention:
Permanent

Characterization of Sorbed Strontium on Monosodium Titanate

Martine C. Duff, Douglas B. Hunter, David T. Hobbs and Samuel D. Fink

REPORT DATE: JULY 25, 2001

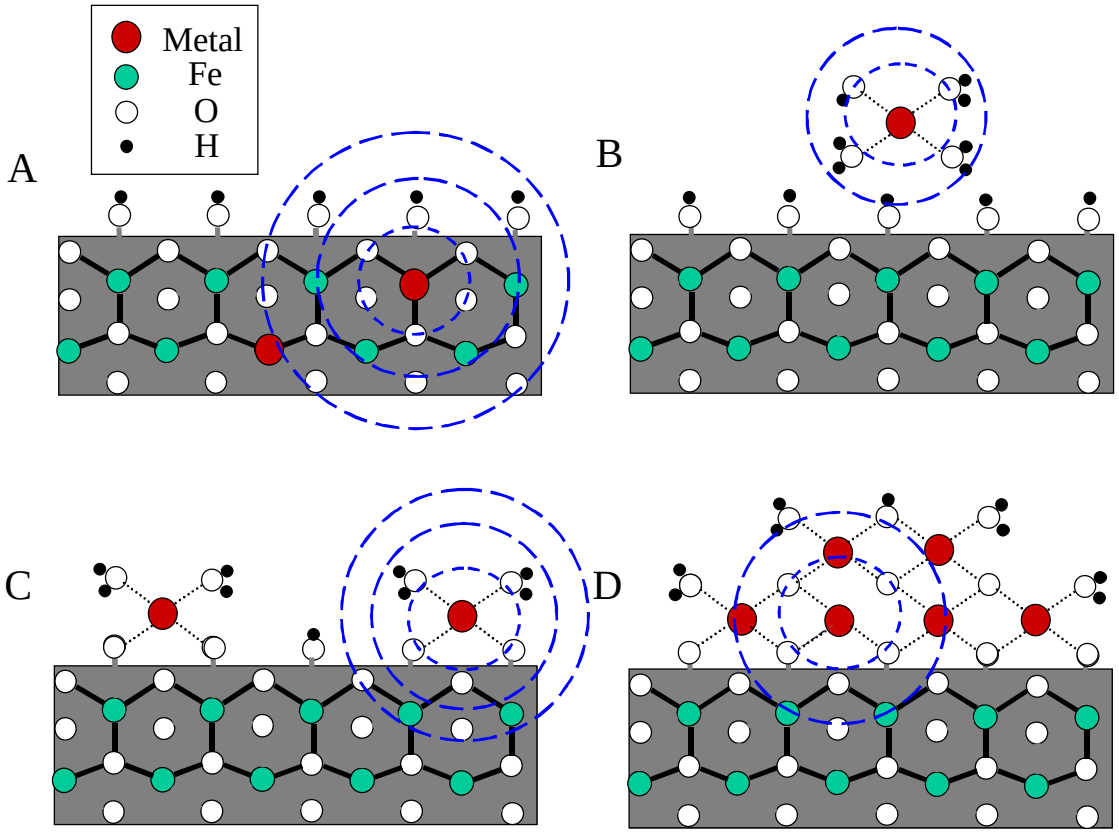

Westinghouse
Savannah River Company
Aiken, SC 29808

Prepared for the U.S. Department of Energy
under Contract Number DE-AC09-96SR18500

REVIEWS AND APPROVALS

M. C. Duff 6/25/01

M. C. Duff, Author, Waste Processing Technology — Date

Douglas B. Hunter 6/25/01

D. B. Hunter, Author, Nonproliferation Technology — Date

D. T. Hobbs 7/9/01

D. T. Hobbs, Author, Waste Processing Technology — Date

Samuel D. Fink 6/25/01

S. D. Fink, Level 4 Manager and TFA Lead Waste Processing Technology — Date

for 6/29/01

R. E. Edwards, Manager, Process Engineering — Date

6/29/01

J. T. Carter, Director of Engineering, SWPF — Date

W L Tamosaitis 6/25/01

W. L. Tamosaitis, Manager, Waste Processing Technology — Date

Major C. Thompson 6/25/01

M. Thompson, Design Check, Actinide Technology — Date

TABLE OF CONTENTS

LIST OF FIGURES iv
LIST OF TABLES vi
ACRONYMS AND ABBREVIATIONS vii
1.0 EXECUTIVE SUMMARY 1
2.0 INTRODUCTION 2
2.1 Uptake Mechanisms of Metals by Surfaces. 2
2.2 Use of XAFS Techniques to Characterize Metal Uptake by Surfaces. 4
2.3 Experimental Objectives. 4
3.0 METHODS AND MATERIALS 5
3.1 Sample Preparation. 5
3.1.1 XANES and EXAFS Data Collection and Analyses. 6
4.0 RESULTS 10
4.1.1 Background on Sr-XAFS Studies with Sr-containing Materials. 10
4.1.2 Sr-XANES Studies with Sr-loaded MST Samples. 13
4.2 EXAFS Analyses. 15
4.2.1 The k^{3}-weighted Chi Data for the Sr Standards and Sr-Loaded MST. 16
4.2.2 Fourier-Transformed Data for the Dilute $SrCl_2$ Solution and Sr^{2+}-loaded MST. 19
4.2.2.1 Higher Shell Fits for Sr-Ti and Sr-O Interactions. 28
4.3 Modeling of Sr^{2+} Sorption on MST 29
4.4 Comparison of First Shell Coordination Data with Literature Findings 30
4.5 Comparison of Second and Third Shell Coordination Data with Literature Findings 32
5.0 DISCUSSION AND CONCLUSIONS 34
5.1 Determination of the Uptake Mechanism 34
5.2 Influence of Sorption Mechanism on Process 34
5.3 The Structure of MST is Unknown 35
5.4 Suggestions for Further Study 35
6.0 ACKNOWLEDGEMENTS 36
7.0 APPENDIX 37
8.0 REFERENCES 41

LIST OF FIGURES

Figure 2-1 Simplified diagram of the types of associations a metal could have with a surface. A) Structural incorporation, B) Outer-sphere (electrostatic) sorption, C) Specific or inner-sphere sorption and D) Surface precipitation. Blue rings denote first, second and third environments that can be probed with XAFS techniques. 3
Figure 3-1 Photograph of the moist Sr^{2+}-loaded MST samples analyzed using XAFS techniques. Sample 1a (left), which had the highest Sr^{2+} loading, is more yellow in color than that of the samples with lower levels of sorbed Sr^{2+} 5
Figure 3-2 Diagram of the downstream portion of the hutch table at NIST beamline X23a2 (not drawn to scale) 7
Figure 3-3 Side view of the downstream portion of the hutch table at beamline X26a. The SiLi detector (light blue item on right of table) was not used in this study (picture kindly provided by A. Lanzirotti, Univ. of Chicago). 8
Figure 3-4 Overhead view of the downstream portion of the hutch table at beamline X26a showing a) the incoming beam with (closed) shutter, b) ion chamber, and c) the sample holder. The pin diode detector used in this study is not shown. (Photo provided by A. Lanzirotti, Univ. of Chicago.) 9
Figure 4-1 Plot of the Sr-XANES data for the Sr^{2+}-loaded MST samples. We obtained the SrMST4 data at beamline X23a2; and acquired the remaining data at beamline X26a. ..14
Figure 4-2 Plot of the Sr-XANES data for two of the Sr^{2+}-loaded MST samples and the two Sr^{2+}-containing solutions. We acquired the SrMST4 data at beamline X23a2 and acquired the remaining data at beamline X26a. 15
Figure 4-3 Plot of the Sr-XANES data for a Sr^{2+}-loaded MST sample and the Sr^{2+}-containing solids. We acquired the data for Sr standards at beamline X26a and acquired data for SrMST4 at beamline X23a2. 15
Figure 4-4 The k^3-weighted chi data (the plot of the wavevector in reciprocal space) for the Sr^{2+}-loaded MST samples. We collected the data at beamline X26A—with the exception of that for SrMST4, which we collected at X23a2. 17
Figure 4-5 The k^3-weighted chi data for Sr^{2+} in $SrCO_{3(s)}$ and $SrHLW_{(aq)}$. We collected the data at beamline X26A. 17
Figure 4-6 The k^3-weighted chi data for Sr^{2+} in $SrTiO_{3(s)}$. We collected the data at beamlines X26a and X23a2. 18
Figure 4-7 The k^3-weighted chi data Sr^{2+} in $Sr(NO_3)_{2(s)}$ We collected the data at beamline X26a. 18
Figure 4-8 FT RDF data for Sr^{2+}-loaded MST samples and the $SrCl_{2(aq)}$ standard. 20
Figure 4-9 FT RDF data and first shell Sr-O model fit data for SrMST1 without the third cumulant term—uncorrected for phase shift. 21
Figure 4-10 FT RDF data and first shell Sr-O model fit data for SrMST1. The third cumulant term was included in the fit—uncorrected for phase shift. 22
Figure 4-11 FT RDF data and first shell Sr-O model fit data for SrMST3 without the third cumulant term—uncorrected for phase shift. 23
Figure 4-12 FT RDF data and first shell Sr-O model fit data for SrMST3. The third cumulant term was included in the fit—uncorrected for phase shift. 24
Figure 4-13 FT RDF data and first shell Sr-O model fit data for SrMST4 without the third cumulant term—uncorrected for phase shift. 25

Figure 4-14 FT RDF data and first shell Sr-O model fit data for SrMST4. The third cumulant term was included in the fit—uncorrected for phase shift. 26
Figure 4-15 FT RDF data and first shell Sr-O model fit data for the dilute $SrCl_2$ solution without the third cumulant term—uncorrected for phase shift. 27
Figure 4-16 Back-transformed chi data and model second and third shell fit data for interactions of Sr-Ti_1, Sr-O_1 and Sr-Ti_2 for Sr^{2+}-loaded SrMST1. 31
Figure 4-17 Back-transformed chi data and model second and third shell fit data for interactions of Sr-Ti_1, Sr-O_1 and Sr-Ti_2 for Sr^{2+}-loaded SrMST3. 31
Figure 4-18 Back-transformed chi data and model second and third shell fit data for interactions of Sr-Ti_1, Sr-O_1 and Sr-Ti_2 for Sr^{2+}-loaded SrMST4. 32
Figure 4-19 EXAFS-based molecular model of association of Sr^{2+} with TiO_6 groups. 33
Figure 4-20 EXAFS-based molecular model of association of Sr^{2+} with corner-shared TiO_6 groups.....33
Figure 7-1 Back-transformed chi data and model fit second shell data for interactions of Sr-O without the C3 term for Sr^{2+}-loaded SrMST1. 37
Figure 7-2 Back-transformed chi data and model fit second shell data for interactions of Sr-O with the C3 term for Sr^{2+}-loaded SrMST1. 37
Figure 7-3 Back-transformed chi data chi data and model fit data for second shell interaction of Sr-Ti without the C3 term for Sr^{2+}-loaded SrMST1.....38
Figure 7-4 Back-transformed chi data and model fit data for second shell interactions of Sr-Ti with the C3 term for Sr^{2+}-loaded SrMST1. 38
Figure 7-5 Back-transformed chi data and model fit data for third shell Sr-O interactions without the C3 term for Sr^{2+}-loaded SrMST1. 39
Figure 7-6 Back-transformed chi data and model fit data for third shell Sr-O interactions with the C3 term for Sr^{2+}-loaded SrMST1. 39
Figure 7-7 Back-transformed chi data and model fit data for interactions of second shell Sr-Ti and third shell Sr-O interactions for Sr^{2+}-loaded SrMST1—without the C3 term. 40

LIST OF TABLES

Table 3-1 The Sr^{2+}-materials that were analyzed with XAFS. The MST solids were equilibrated for 1 week with the target metal. 5
Table 3-2 Reference Sr^{2+} materials used as standards for the XAFS analyses. 6
Table 4-1 Literature XAFS fit data for solid phase of Sr^{2+}. The magnitude of the Debye-Waller Factor [σ^2[Å]^2] indicates the variation in the bond length determination. 11
Table 4-2 First coordination shell Sr-O fit literature data for dissolved Sr^{2+}. The magnitude of the Debye-Waller Factor [represented in as σ^2[Å]^2] indicates the variation of the bond length determination. 12
Table 4-3 Fit results for a first shell Sr-O interaction with and without the third cumulant (C3) term for the Sr^{2+} sorbed MST samples. Use of the third cumulant term in the fits for Sr in the dilute $SrCl_{2(aq)}$ solution yielded no differences (in CN or R). Fits for SrMST2 were not performed due to insufficient data quality. DeltaR and deltaCN represent the change in R and CN values (respectively) with the inclusion of the C3 term. The magnitude of the Debye-Waller Factor [represented in as σ^2[Å]^2] indicates the variation of the bond length determination (or spread but not error). It also provides information on goodness of fit—for example, a negative value would indicate a poor fit. A decrease in the D-W factor with inclusion of the C3 term signifies that there is less variance and hence better fit. Addition of the third cumulant (C3) term in the fit accounts for the anharmonicity arising from weak back-scatterers. The addition of this C3 variable in the fitting process should result in a smaller D-W factor. Without the C3 term, the D-W factor is overestimated. 28
Table 4-4 Fit results for a second and third shell Sr interactions with and without the third cumulant (C3) term for the Sr^{2+} sorbed MST samples. Use of the third cumulant term in the fits for Sr in the dilute $SrCl_{2(aq)}$ solution yielded no differences (in CN or R). The third cumulant term was not included in fits for second and third shell interactions due to a limited number of degree of freedom, which did not allow addition of another floating variable. Fits for SrMST2 were not performed due to insufficient data quality. 30

ACRONYMS AND ABBREVIATIONS

CN	Coordination number
$\delta(K)$	Electronic phase shifts due to atomic potentials
EXAFS	Extended X-ray Absorption Fine-Structure
E	E is the kinetic energy of the photoelectron
E_0	EXAFS defined edge energy in electron volts or eV (not equal to edge energy as defined by XANES but is equal to the energy of the photoelectron at $k = 0$.
E_0 Shift	A relative value of E_0 (a variable in the EXAFS Equation)
F	Backscattering amplitude of the atom
FEFF	An automated computer program for making *ab initio* multiple scattering calculations of XAFS and XANES spectra for atoms.
FeOOH	The Fe(III)-oxide mineral goethite.
FFIT	A Levenberg-Marquardt fitting program created by researchers at the University of Washington
FT	Fourier-transform
$\hbar$	Plank's constant
HLW	High Level Waste
HFO	Hydrous ferric oxide.
HMO	Hydrous manganese oxide.
k	Chi where k is the square root of $[(2m / \hbar^2) * (E - E_0)]$
m	Mass of the photoelectron
MST	Monosodium titanate
NSLS	National Synchrotron Light Source
O	Oxygen
R-space	R-space pertains to mean atom position or bond distance (radial distance in Å)
RDF	Radial Distribution Function
RT	Room Temperature.
S/N	Signal to Noise
S0ˆ2 or S_0^2	Amplitude reduction factor (EXAFS Equation variable associated with central atom shake-up and shake-off effects)
σ^2 or SIGMA^2	Debye-Waller Factor or Relative Mean Square Disorder in bond length (a variable in the EXAFS Equation)
Si(Li)	An energy dispersive Li-doped silicon detector
Sr	Strontium
SRTC	Savannah River Technology Center
Ti	Titanium
WSRC	Westinghouse Savannah River Company
XAFS	X-ray Absorption Fine-Structure (XANES plus EXAFS)
XANES	X-ray Absorption Near-Edge Structure
XRD	X-ray Diffraction

1.0 EXECUTIVE SUMMARY

Approximately 130 million L of High-Level Radioactive Waste (HLW, the waste product associated with the dissolution of spent fuel rods for the recovery of plutonium) material reside in carbon steel subsurface tanks awaiting treatment at the Savannah River Site (SRS). The currently proposed designs for the Salt Processing Facility at the SRS include use of monosodium titanate (MST) to remove the strontium (Sr) and actinides from the HLW. Solid phases such as the titanates have a strong affinity for dissolved Sr^{2+} and actinides under conditions relevant to processing of highly alkaline HLW salt solutions but the mechanism of Sr uptake by MST is not known. Although the salt solutions contain high levels of Na^{+} (several M) which is a potential competitor with Sr^{2+} for sorption sites on MST, Sr^{2+} is preferred over Na^{+} by MST—despite the high levels of (background) Na^{+}. This preference for Sr^{2+} is not understood and the structure of MST is not known. Uptake processes of dissolved species by solids can occur by several mechanisms: structural incorporation, ion exchange (electrostatic or outer-sphere) sorption, specific adsorption and surface precipitation. Fundamental information about the mechanism of uptake will provide a better understanding about processing with MST, such as washing after Sr^{2+} and actinide removal. This report discusses the characterization of the nature of Sr^{2+} sorption on MST in HLW salt solutions. The study used X-ray absorption fine-structure spectroscopy (XAFS) to characterize the chemistry of Sr^{2+} on MST yielding the following conclusions.

- The speciation of sorbed Sr^{2+} on MST does not change over the range of surface Sr^{2+} loadings examined in this study.

- The Sr^{2+} undergoes partial dehydration upon sorption to MST.

- Presence of Ti in the second coordination shell of the Sr^{2+} on the MST suggests that specific adsorption is the predominant mechanism and that electrostatic bonding (also known as ion exchange of hydrated surface-associated species such as dissolved Na^{+}) in the electric double-layer of the HLW salt simulant solution does not occur.

- Some structural incorporation of Sr^{2+} (as a replacement for structural Na^{+}) may occur but there are not enough Ti atoms in the second shell to suggest that this is the primary mechanism of uptake.

- Interpretations of the EXAFS data and EXAFS-based molecular modeling suggest Sr^{2+} may associate with more than one TiO_6 octahedra (assuming the presence of Ti octahedra because the structure of MST is not known) as a partially aquated ion.

- The speciation of sorbed Sr^{2+} on MST was not like that of Sr^{2+} in the HLW salt simulant solution, suggesting that a change in the Sr^{2+} coordination environment occurs upon sorption to MST.

2.0 INTRODUCTION

Solid phases such as the titanates have a strong affinity for dissolved Sr^{2+} and actinides under conditions relevant to the processing of highly alkaline HLW salt solutions. These sorptive materials are being considered for use in HLW treatment to concentrate dissolved forms of radiostrontium and actinides. Removal and retention of dissolved species by reactive surface does not always involve "sorption"—even in the most general sense. We will discuss how our study findings relate to process chemistry and engineering in the Discussion and Conclusions section of this report but first we will discuss four mechanisms of metal uptake by surfaces and the use of XAFS spectroscopic methods elucidate the coordination and bonding environment of those metals.

2.1 Uptake Mechanisms of Metals by Surfaces.

Uptake processes by solids can occur by several mechanisms: structural incorporation, ion exchange (electrostatic or outer-sphere) sorption, specific adsorption and surface precipitation. A schematic of these processes is shown in **Figure 2-1**. Many of these terms have been used loosely in the literature and their use varies with scientific discipline. Our presentation focuses on the surface and its interaction with the sorbing solution species. A more thorough review of these processes is presented elsewhere.[1,2] Expression of these uptake processes can depend on the amount of metal added, solution and solid phase characteristics.

"Ion exchange" can have different meanings, which results in some confusion in the literature. One very general way to express ion exchange is *structural incorporation,* which is the substitution of a solution species for a structural atom:

$$CaCO_{3(s)} + Sr^{2+} \rightleftharpoons SrCO_{3(s)} + Ca^{2+}$$

This type of sorption typically requires ready access to structural atoms. Another example of this process would be the exchange of the structural Na^{+} in monosodium titanate (MST) with Sr^{2+}. Although little is known about the structure of MST, access (for Sr^{2+}) could occur within long sheets of edge linked TiO_6 octahedra that contain Na^{+} ions. In this case, the structural incorporation of Sr^{2+} in MST would result in the presence of several Ti atoms in the second coordination shell of the Sr^{2+}. Ideally, structural incorporation of the Sr^{2+} should also result in a similar number of first shell oxygen atoms to that of the replaced ion prior to its release. Therefore, the local environment of the exchanged atom would resemble the environment the newly exchanged atom had prior to its release (**Figure 2-1**).

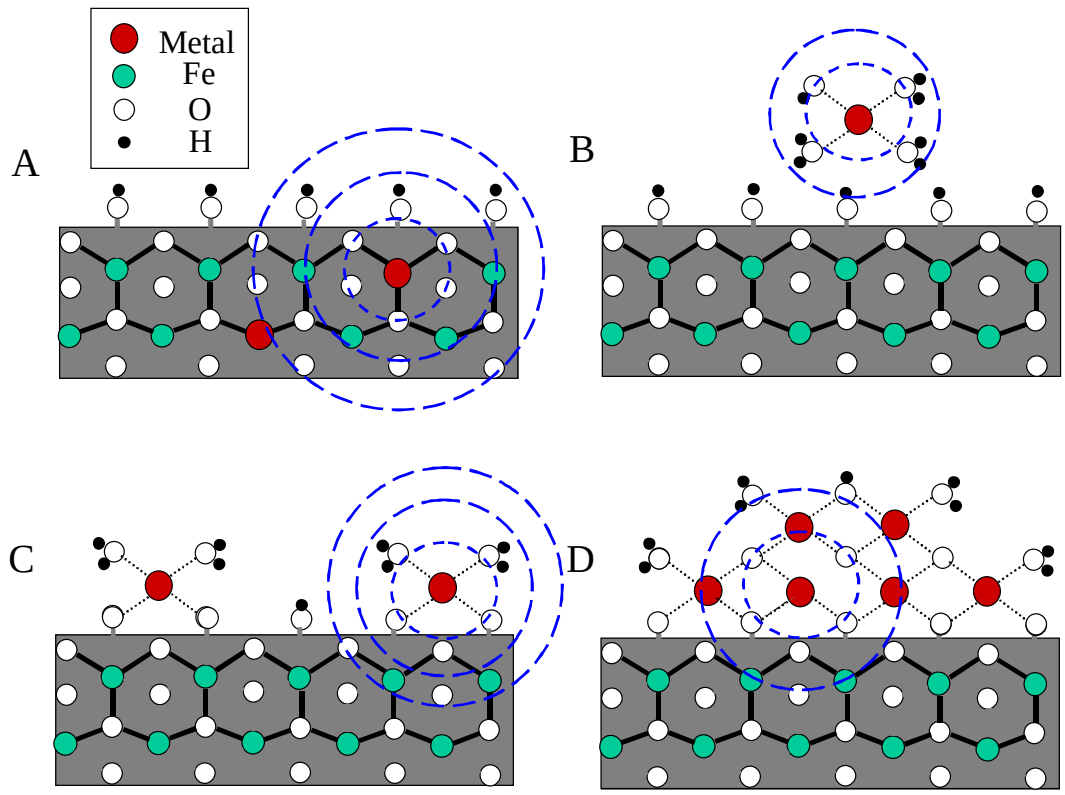

Figure 2-1 Simplified diagram of the types of associations a metal could have with a surface. A) Structural incorporation, B) Outer-sphere (electrostatic) sorption, C) Specific or inner-sphere sorption and D) Surface precipitation. Blue rings denote first, second and third environments that can be probed with XAFS techniques.

Ion exchange in a more restrictive sense is an electrostatic process involving the replacement of a one readily exchangeable hydrated ion by another similarly exchangeable ion (**Figure 2-1**). This type of sorption is also referred to as *outer sphere* sorption. Ion exchange does not involve the formation of bonds on the participating surface because the sorbed ion is present in the diffuse double layer (DDL). This type of sorption is normally reversible[3] and is a function of ionic strength. At high ionic strengths, the DDL collapses and less sorption by ion exchange is observed than at low ionic strengths. Ion exchange sorption is often associated with materials that have constant surface charge and exhibit no change in overall surface charge upon ion exchange sorption. An example of this process would be exchange of hydrated Na^+ ion for hydrated Sr^{2+} in the DDL.

Specific adsorption involves the formation of predominantly covalent bond with the surface, but the bond can have some ionic behavior. This type of sorption is often referred to as *chemisorption* or *inner sphere* sorption. Specifically adsorbed metals often contain one or more atoms from the participating surface in the second coordination shell (**Figure 2-1**). This type of sorption involves the release of H^+ or structural surface ions (such as Na^+ in MST) upon sorption. For example, specific sorption of Sr^{2+} to MST could result in the

presence of Ti atoms in the second coordination shell of the Sr^{2+}. Specific adsorption is usually irreversible.[3]. However, in the literature, specific adsorption is rarely differentiated from structural incorporation or surface precipitation. Specific adsorption may involve mononuclear complexes or polymeric species. Specific adsorption is influenced by other solution- and surface-related variables.[4]

Surface Precipitation occurs by nucleation of new solid phase on a host surface (**Figure 2-1**). For example, when the concentration of a dissolved metal such as Sr^{2+} is high enough to result in the super-saturation of one or more Sr^{2+}-containing phase [such as $SrCO_{3(s)}$] in the presence of MST, the MST facilitates the nucleation of the new solid Sr^{2+}-rich phase. Surface precipitation of Sr^{2+} would result in existence of second shell Sr^{2+} atoms around each Sr^{2+}.

2.2 Use of XAFS Techniques to Characterize Metal Uptake by Surfaces.

The environment of metals associated with surfaces can be investigated with analytical techniques such as X-ray absorption fine-structure (XAFS) spectroscopy. We will use Sr-XAFS to study the environment of the sorbed Sr^{2+}. To determine the nature of metal sorption on MST, the XAFS studies will use with solids that have a range of Sr^{2+} loadings in a HLW salt simulant solution. The XAFS spectroscopic techniques are among the best for providing detailed chemical speciation information in environmental samples—particularly when information from multiple characterization techniques is available. The term XAFS is applies to X-ray absorption near-edge structure (XANES) and extended X-ray absorption fine-structure (EXAFS) spectroscopic techniques. The XAFS spectra give robust local structural information on coordination number (CN), bonding symmetry, neighbor and near-neighbor atomic distances and bond disorder (as the root mean square deviations of distances about the average values). Additionally, the information gained is atom specific—making it a versatile technique for structural determinations of atom clusters.[5,6]

The XANES techniques involve *multiple* scatterings of an ejected photoelectron with moderate kinetic energy with neighboring atoms. Unlike EXAFS, for XANES the ejected photoelectron does not enter the continuum.[5] The XANES spectroscopic techniques can provide information on the local coordination environment and oxidation state of the metal of interest.[5] The EXAFS spectroscopy in particular has been quite successfully applied to the structural elucidation of metals clusters and sorbed metals on surfaces because the technique does not require long range order (i.e., periodicity) or crystalline samples.

2.3 Experimental Objectives.

The primary objective of this research was to obtain information on speciation of Sr^{2+} after reaction with MST in highly alkaline HLW simulant solutions. Prior to this preliminary study, little information was available on the speciation of sorbed Sr^{2+} on these materials. Several metal-loaded MST samples were prepared to have a range of metal loadings. We used XAFS techniques to obtain information on the average local structural speciation of the sorbed Sr^{2+} and actinides such as CN, geometry, near and next-nearest neighbor environment of the target metals.

3.0 METHODS AND MATERIALS

Samples were prepared for XAFS analyses. The details of the sample preparation, XAFS data collection and data analyses are presented below.

3.1 Sample Preparation.

A synthetic HLW salt solution was made of 1.33 M NaOH, 2.6 M $NaNO_3$, 0.43 $Na(AlO_4)_2$ 0.34 M $NaNO_2$, 0.52M $NaSO_4$ and 0.026 M $NaCO_3$. One liter of the HLW salt solution was allowed to equilibrate with MST (amounts listed in **Table 3-1**) for a one week period. The samples were filtered with a 0.45-µm polycarbonate filter. The solids were placed in 3-mL microcentrifuge tubes as shown in **Figure 3-1** with a small amount of salt solution. Several reference materials were prepared for XAFS analyses (**Table 3-2**).

Table 3-1 The Sr^{2+}-materials that were analyzed with XAFS. The MST solids were equilibrated for 1 week with the target metal.

Treatment Name	Sr^{2+} Concentration Added	Solid Amount (g)	Loading (mg kg^{-1})
SrMST1	1 mg Sr^{2+} L^{1}	0.1	9000
SrMST2	1 mg Sr^{2+} L^{1}	0.2	4500
SrMST3	1 mg Sr^{2+} L^{1}	0.5	1800
SrMST4	1 mg Sr^{2+} L^{1}	1.0	900

Figure 3-1 Photograph of the moist Sr^{2+}-loaded MST samples analyzed using XAFS techniques. Sample 1a (left), which had the highest Sr^{2+} loading, is more yellow in color than that of the samples with lower levels of sorbed Sr^{2+}.

Table 3-2 Reference Sr^{2+} materials used as standards for the XAFS analyses.

Reference Material	Description
$SrCl_{2(aq)}$	10^{-6} M Sr^{2+} in de-ionized water (added as $SrCl_2$)
$SrHLW_{(aq)}$	10^{-6} M Sr^{2+} in MST-free HLW salt solution (added as $SrCl_2$)
$SrTiO_{3(s)}$	Commercially available nanosized solid
$SrCO_{3(s)}$	Commercially available solid
$Sr(NO_3)_{2(s)}$	Equilibrated for 45 C for 24 hours and filtered.

3.1.1 XANES and EXAFS Data Collection and Analyses.

The Sr-XAFS data were collected at the Sr K-edge (16.105 keV) on moist filtered MST solids and reference materials (**Table 3-1; Table 3-2**). The Sr-XAFS data were collected on beamline X23a2 (schematic shown in **Figure 3-2**) and beamline X26a (schematics shown in **Figure 3-3**; Error! Reference source not found.) at the National Synchrotron Light Source (NSLS, Brookhaven National Laboratory, Upton, NY). The XAFS data were collected in transmission and fluorescence mode using an unfocussed X-ray beam and a fixed-exit Si(311) monochromator (X23a2) or channel-cut Si(111) monochromator (X26a). Ion chambers were used to collect incident (*Io*) and transmission (*It*) signals at X23a2 whereas an ion chamber was used to collect *Io* signals and a pin diode was used to measure *It* at X26a. Simultaneous data collection of a reference (*Ir*) signal was not feasible because the samples absorption of the X-ray beam was substantial. Gas ratios for the data collection in *Io* were 100% Ar. A Lytle detector was used to collect fluorescence X-rays (*If*), using an Al metal foil to reduce the background fluorescence counts. The monochromator energy (X23a2) was maximized using a piezo stack feedback energy stabilization system, with a settling time of 0.3 seconds per change in monochromatic energy. Monochromator energy maximization was not required at beamline X26a. An X-ray beam size of 2 by 28 mm^2 (X23a2) or 350 μm^2 (X26a) was used.

Background contribution to the EXAFS spectra was removed using an algorithm (AUTOBK) developed by Newville et al. (1993), which minimizes R-space values in low *k*-space. Each chi data set was read into the WINXAS analysis package.[7,8] Replicate scans were co-added (that is the spectra were summed and divided by the number of scans) to improve S/N. After background subtraction and normalization, the XANES spectra were compared with spectra from the Sr standards and spectra from the literature. For the MST samples and most of the Sr reference materials, the Sr-EXAFS spectra were analyzed from 2 to 14 $Å^{-1}$. The $SrCO_3$ and $Sr(NO_3)_2$ standards were analyzed from 2 to 11 $Å^{-1}$. Chi data were k^3-weighted. The chi data were Fourier-transformed (FT) to yield R-space or Radial Distribution Function (RDF) plots.[9] The EXAFS spectra that were acquired for the Sr^{2+} references were used to estimate phase shifts, coordination environment and radial bond distances. Simulated EXAFS spectra were also generated based on the documented crystallographic properties for Sr^{2+} using *ab initio* based theory, which involved FEFF 7.2, a program created by researchers at the Univ. of Washington.[10,11,12,13,14,15]

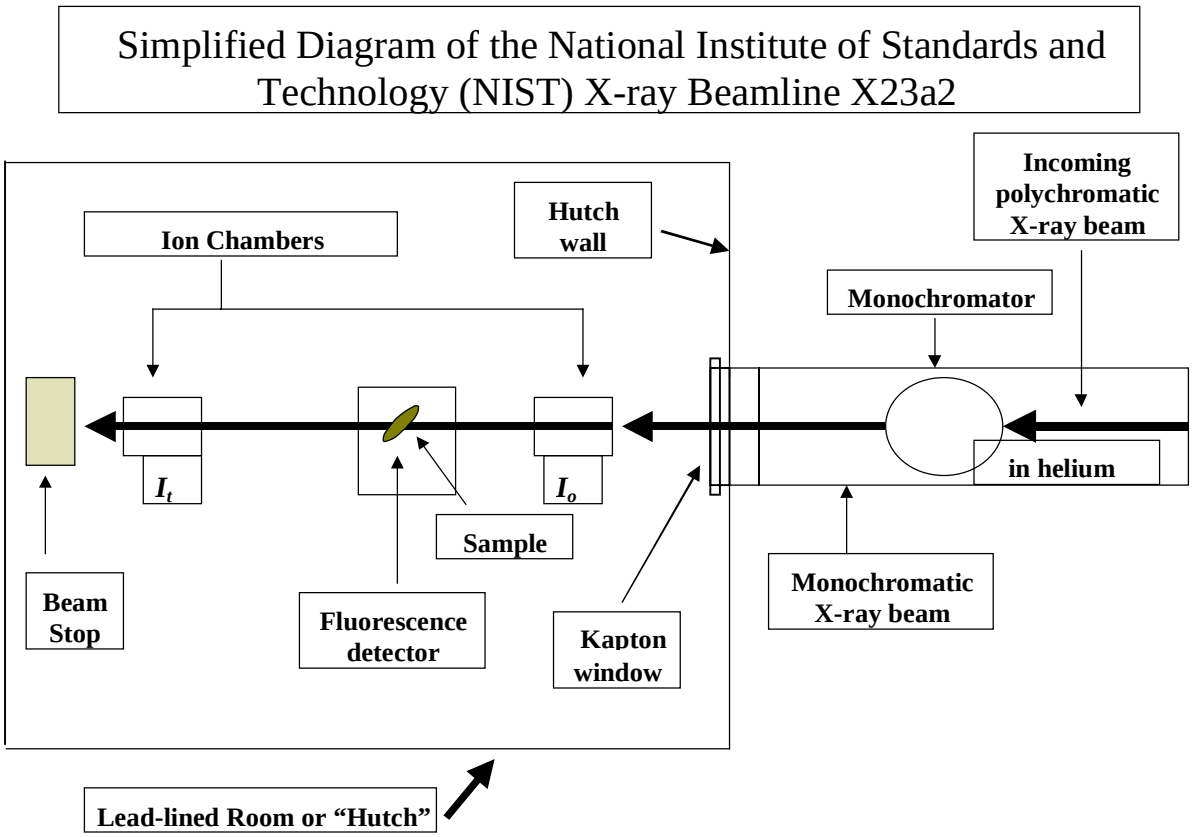

Figure 3-2 Diagram of the downstream portion of the hutch table at NIST beamline X23a2 (not drawn to scale).

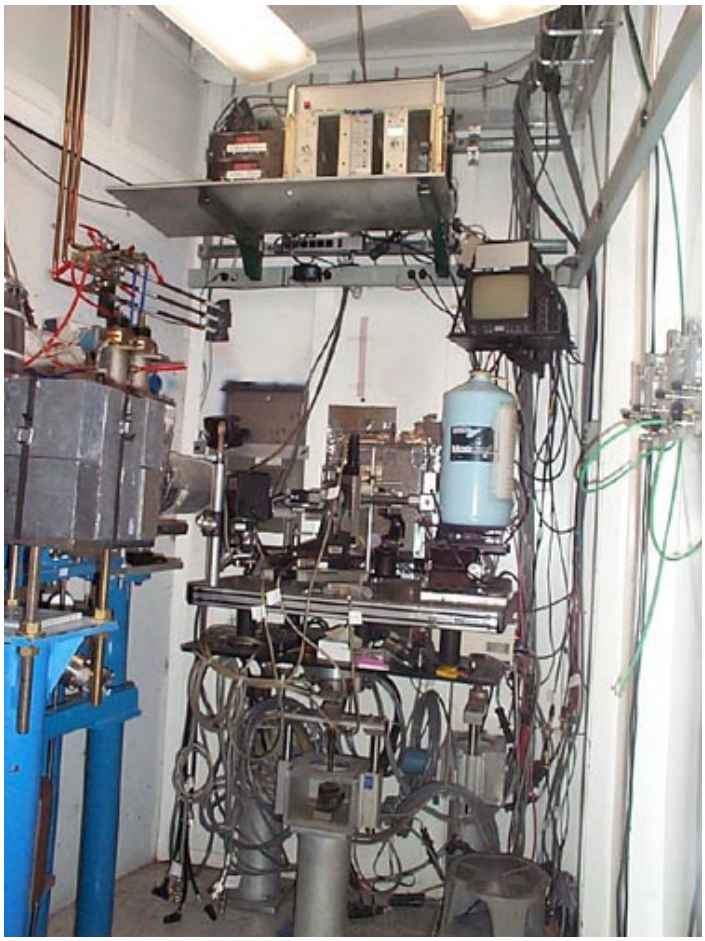

Figure 3-3 Side view of the downstream portion of the hutch table at beamline X26a. The SiLi detector (light blue item on right of table) was not used in this study (picture kindly provided by A. Lanzirotti, Univ. of Chicago).

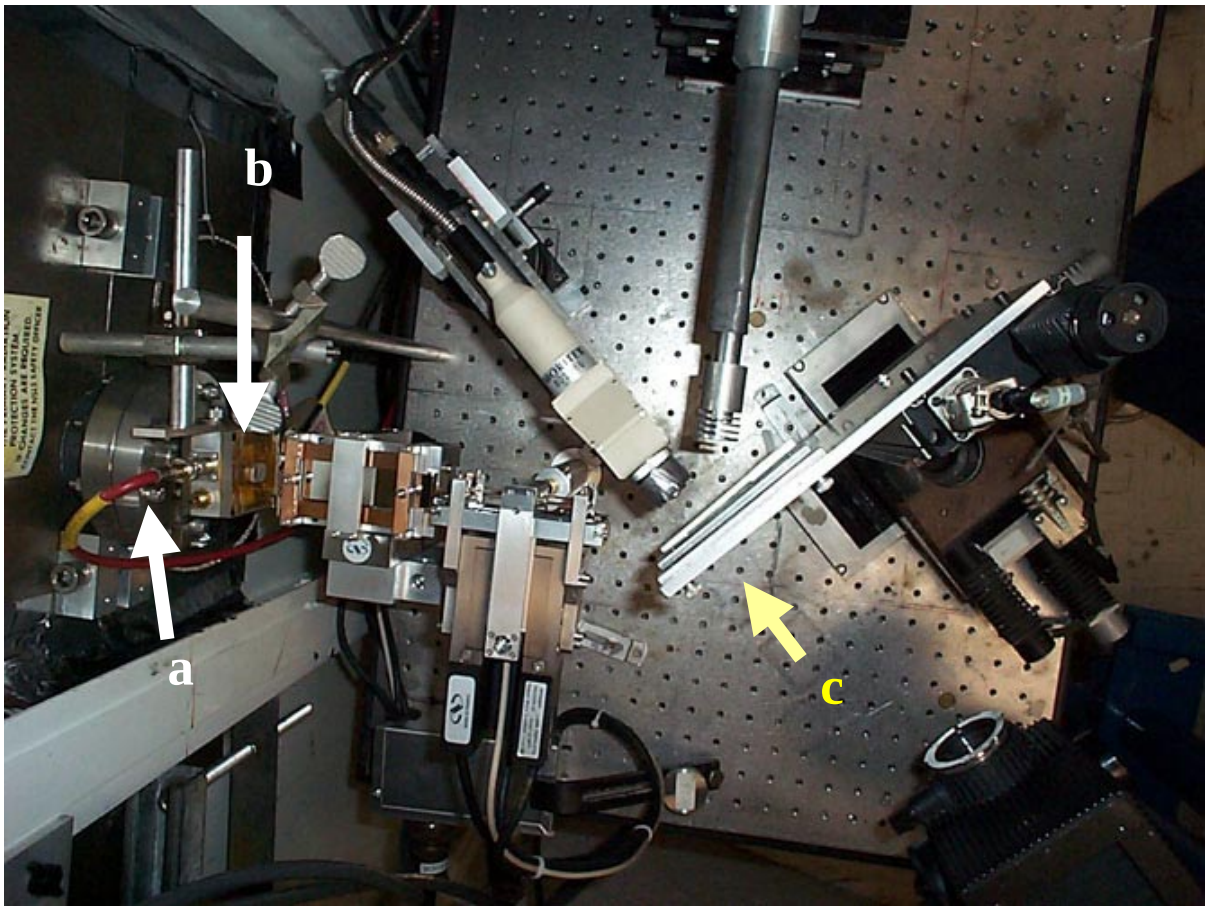

Figure 3-4 Overhead view of the downstream portion of the hutch table at beamline X26a showing **a**) the incoming beam with (closed) shutter, **b**) ion chamber, and **c**) the sample holder. The pin diode detector used in this study is not shown. (Photo provided by A. Lanzirotti, Univ. of Chicago.)

4.0 RESULTS

4.1.1 Background on Sr-XAFS Studies with Sr-containing Materials.

Strontium K-edge XANES and XAFS techniques have been applied to study the bonding environment of sorbed, solution and solid phase Sr^{2+} species.[16,17,18,19,20] Strontium-XANES studies have been performed with Sr^{2+}-rich carbonates and Sr^{2+}-containing silicates and the interpretations of spectra from sample treatments are generally qualitative.[20] This is because solution and solid phase Sr^{2+} species are typically present in the +II oxidation state and large energy shifts for the XANES edge of Sr^{2+} are usually not observed. However, ligand and coordination effects are observed and some comparisons can be made between the XANES spectra from the unknowns and that of the characterized reference materials of known coordination and bonding environment.[20]

Table 4-1 provides a summary of the Sr-XAFS data obtained from a review of these studies. Some of the EXAFS studies that have characterized the environment of sorbed Sr^{2+} on hydrous oxides of Fe and Mn observe a metal in the second coordination shell.[16,17] Because a metal was found in the second coordination environment, these studies refer to the nature of the sorption as being due to the ion exchange of hydrated Sr^{2+} (Note: This conclusion is not consistent with the previous section that describes ion exchange in the strict sense.[16,17] These studies also report that they could fit Sr or Fe in the second shell over a range of surface Sr^{2+} loadings and hence, these data present great confusion and about the quality of the XAFS data and the data analyses.[21] In contrast, other sorption studies with Sr^{2+} sorbed on the FeOOH (goethite) do not observe a metal in the second coordination shell and conclude that outer sphere adsorption is operative.[19] Extreme caution should be used when EXAFS studies are used to determine the nature of the sorption (such as ion exchange vs. specific adsorption, as described in O'Day et al. (2000).

O'Day et al. (2000) and Sahai et al. (2000) reviewed the use of Sr-EXAFS to characterize atomic structural properties of Sr^{2+} in solutions, in solids and on surfaces. They indicate the literature vary considerably due to the hydrated nature of the large divalent cation (Sr^{2+}).[18,19] This behavior is mainly attributed to differences in experimental EXAFS fitting techniques associated with the determination of amplitude reduction factors, anharmonic disorder and the number of experimental shells included in the model fits. Additionally, some XAFS studies may not account for problems associated with light atom back-scattering. O'Day et al. (2000) and others have included a third cumulant term (C3) in their fits for first shell Sr-O interactions to account for anharmonicity among light back-scattering atoms Sr and O in aqueous environments.[16,17, 18,19] For our studies, we will compare the results of our first shell Sr-O fits with and without the C3 term. It is our opinion that the reports that have excluded the C3 term during the data analyses are in error. This term is important because of the hydrated nature of Sr^{2+} in solution. Exclusion of fitting with the C3 term is most common in the older literature.

Table 4-1 Literature XAFS fit data for solid phase of Sr^{2+}. The magnitude of the Debye-Waller Factor [σ^2[Å]^2] indicates the variation in the bond length determination.

Sample	Interaction	CN	Distance R[Å]	σ^2[Å]^2
$Sr(II)CO_{3(s)}$ [16]	Sr-O	12.96	2.69	0.013
$Sr(II)CO_{3(s)}$ [18]	Sr-O	9	2.61	0.0136
	Sr-C	3	3.05	0.0073
	Sr-Sr	4	4.14	0.0083
	Sr-Sr	2	4.29	0.0063
	Sr-Sr	4	4.92	0.0150
$Sr(II)CO_{3(s)}$ [20]	Sr-O	9	2.59	0.016
	Sr-C	3	3.05	0.014
	Sr-C	3	3.41	0.039
	Sr-Sr	2.6	4.01	0.002
	Sr-Sr	6	4.16	0.028
	Sr-Sr	6	4.91	0.029
$Sr(II)CO_{3(s)}$ at RT [22]	Sr-O	9	2.61	0.0099
$Sr(II)CO_{3(s)}$ [23]	Sr-O	9.2	2.63	0.016
	Sr-C	3.4	3.10	0.010
	Sr-C	1.9	3.45	0.006
	Sr-Sr	2.6	4.01	0.002
	Sr-Sr	1.3	4.15	0.009
	Sr-Sr	2.6	4.17	0.004
	Sr-Sr	1.0	4.93	0.002
$Sr(II)TiO_3$ (cubic) at RT [18]	Sr-O	12	2.72	0.0186
	Sr-Ti	6	3.39	0.0080
	Sr-Sr	6	3.92	0.0121
	Sr-O	24	4.78	0.0066
Sr^{2+} Sorbed on Kaolinite at 14 K [19]	Sr-O	9.9	2.62	0.0082
Sr^{2+} Sorbed on Kaolinite at 14 K [20]	Sr-O	7.5	2.56	0.014
Sr^{2+}-rich Zeolite (Heulandite) RT [18]	Sr-O	8	2.60	0.0144
	Sr-Al/Si	2	3.49	0.0139
	Sr-Al/Si	2	4.14	0.0167
Sr^{2+} Sorbed on Goethite (FeOOH) at RT (low loading) [19]	Sr-O	8.2	2.58	0.00116
Sr^{2+} Sorbed on FeOOH at RT (high loading) [19]	Sr-O	8.3	2.58	0.0140
	Sr-C	0.4	3.03	0.0073
	Sr-Sr	3.1	4.13	0.0090
	Sr-Sr	1.5	4.30	0.0060
	Sr-Sr	No data	No data	>0.025

Table 4-1 Literature XAFS fit data for solid phase of Sr^{2+}. The magnitude of the Debye-Waller Factor [σ^2[Å]^2] indicates the variation in the bond length determination.

Sample Type	Interaction	CN	Distance r[Å]	σ^2[Å]^2
Sr^{2+} Sorbed on FeOOH at RT, pH 9.2[23]	Sr-O	8.0	2.61	0.012
Sr^{2+} Sorbed on FeOOH at RT, pH 10.2[23]	Sr-O	8.2	2.61	0.012
	Sr-Fe	1.8	4.29	0.011
Sr^{2+} Sorbed on HFO, 300°K (low loading) [16,21]	Sr-O	10.49	2.61	0.0098
	Sr-Fe	1.26	3.75	0.0061
Sr^{2+} Sorbed on HFO, 300°K (low loading) [16,21]	Sr-O	12.62	2.64	0.015
	Sr-Sr	11.76	3.45	0.037
Sr^{2+} Sorbed on HFO, 300°K (high loading) [16,21]	Sr-O	12.06	2.61	0.015
	Sr-Fe	2.52	3.40	0.034
Sr^{2+} Sorbed on HFO, 300°K (high loading) [16,21]	Sr-O	12.06	2.61	0.010
	Sr-Sr	2.52	3.40	0.034
Sr^{2+} Sorbed on HMO, RT (low loading) [17,21]	Sr-O	9.54	2.61	0.012
	Sr-Mn	3.70	4.21	0.025
Sr^{2+} Sorbed on HMO, RT (low loading) [17,21]	Sr-O	9.97	2.61	0.013
	Sr-Sr	3.63	3.89	0.015
Sr^{2+} Sorbed on HMO, RT (moderate loading)[17,21]	Sr-O	10.60	2.55	0.014
	Sr-Mn	3.93	4.07	0.029
Sr^{2+} Sorbed on HMO, RT (moderate loading)[17,21]	Sr-O	12.25	2.54	0.018
	Sr-Sr	10.12	3.81	0.036
Sr^{2+} Sorbed on HMO, RT (high loading) [17,21]	Sr-O	11.26	2.56	0.017
	Sr-Mn	5.46	4.14	0.034
Sr^{2+} Sorbed on HMO, RT (high loading) [17,21]	Sr-O	12.18	2.57	0.019
	Sr-Sr	5.46	4.14	0.044
Sr^{2+} Sorbed on Silica at RT [19]	Sr-O	9.7	2.57	0.013

Table 4-2 First coordination shell Sr-O fit literature data for dissolved Sr^{2+}. The magnitude of the Debye-Waller Factor [represented in as σ^2[Å]^2] indicates the variation of the bond length determination.

Sample Type	Interaction	CN	Distance r[Å]	σ^2[Å]^2
0.0001 M $SrCl_{2(aq)}$ [20]	Sr-O	9	2.61	0.030
0.0001 M $SrCl_{2(aq)}$ [18]	Sr-O	9-10	2.65	0.011
0.2 M Sr at RT [24]	Sr-O	7.3	2.62	0.0009
0.2 M $Sr(NO_3)_{2(aq)}$ [24]	Sr-O	7.3	2.62	Not reported

O'Day et al. (2000) examined the environment of Sr^{2+} in zeolite (heulandite) cavities and observed Sr^{2+} existed as a hybrid-like species that maintains a partially-hydrated coordination sphere as well as has Si/Al in the second coordination shell.[18] These data indicate that Sr^{2+} is sorbs as a hydrated species and forms a bond with the zeolite surface in Ca^{2+} (B-channel) sites. There are two other types of cavities/channels in the heulandite, which contain Na^{+} and K^{+} sites but the Sr-EXAFS data indicate that the Sr-O bond distances are either too short or too long to accommodate the sorption of a hydrated Sr^{2+} species at these other sites.

4.1.2 Sr-XANES Studies with Sr-loaded MST Samples.

The XANES spectra are typically used to provide information on the average oxidation state of the element of interest. In HLW salt solutions, oxidation state information for Sr is not of concern because solution Sr is found as the Sr^{2+} species. No reduction-oxidation reactions that could influence the valence of Sr are likely under the conditions of this study. However, Sr-XANES analyses will be conducted because these studies can provide useful information on the structural environment of the element of interest. Small shifts (a few eV) in XANES absorption edge energies can occur when a metal undergoes a change in average oxidation state. As noted in the methods, the XAFS data were taken at beamlines X23a2 and X26a. The origin of the data is presented in the following figures or in figure captions.

The Sr-XANES data for the Sr^{2+}-loaded MST solids studies are shown in **Figure 4-1**. These XANES data indicate that the samples are similar. They also resemble that of the solution Sr^{2+} (**Figure 4-2**). However, the XANES spectra for the samples do not resemble that of solid phase Sr^{2+} standards as shown in **Figure 4-3**.[25] This is evidenced by the difference in such features as white-line maxima and the position of the post edge oscillations.

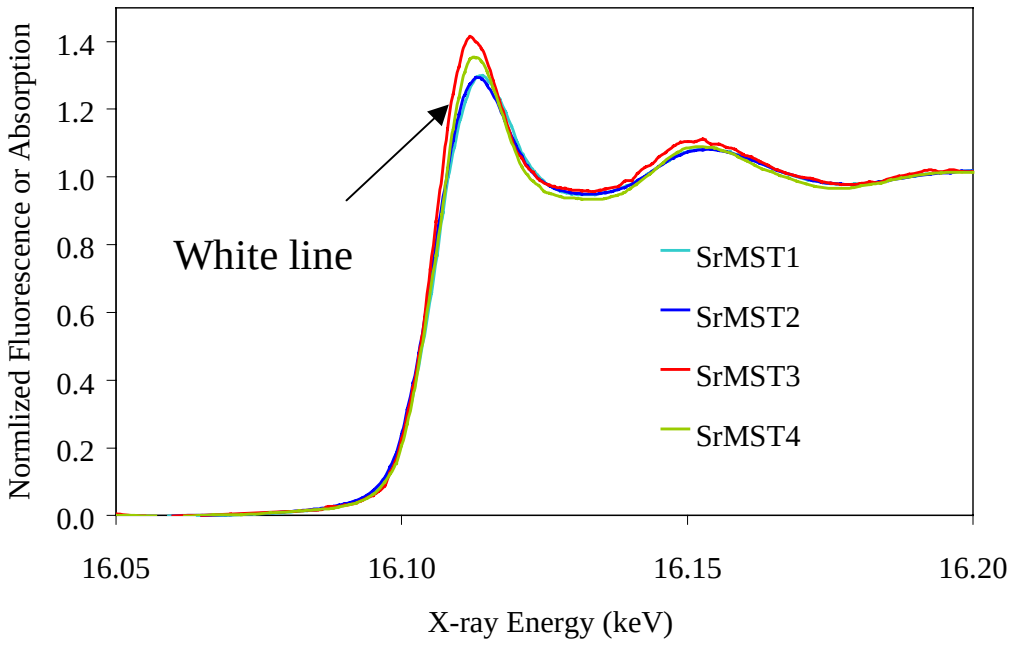

Figure 4-1 Plot of the Sr-XANES data for the Sr^{2+}-loaded MST samples. We obtained the SrMST4 data at beamline X23a2; and acquired the remaining data at beamline X26a**.**

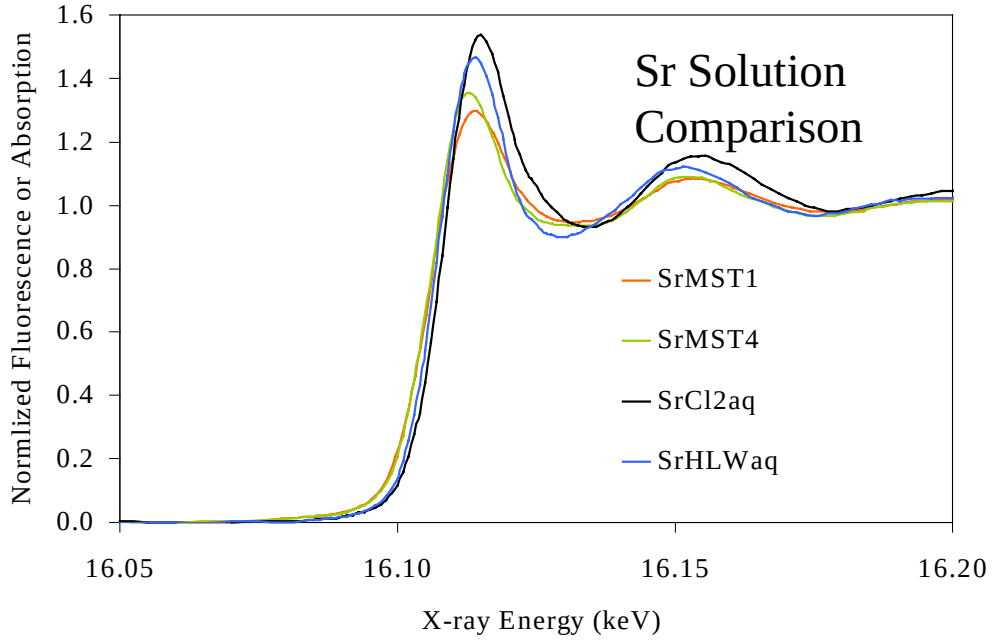

Figure 4-2 Plot of the Sr-XANES data for two of the Sr^{2+}-loaded MST samples and the two Sr^{2+}-containing solutions. We acquired the SrMST4 data at beamline X23a2 and acquired

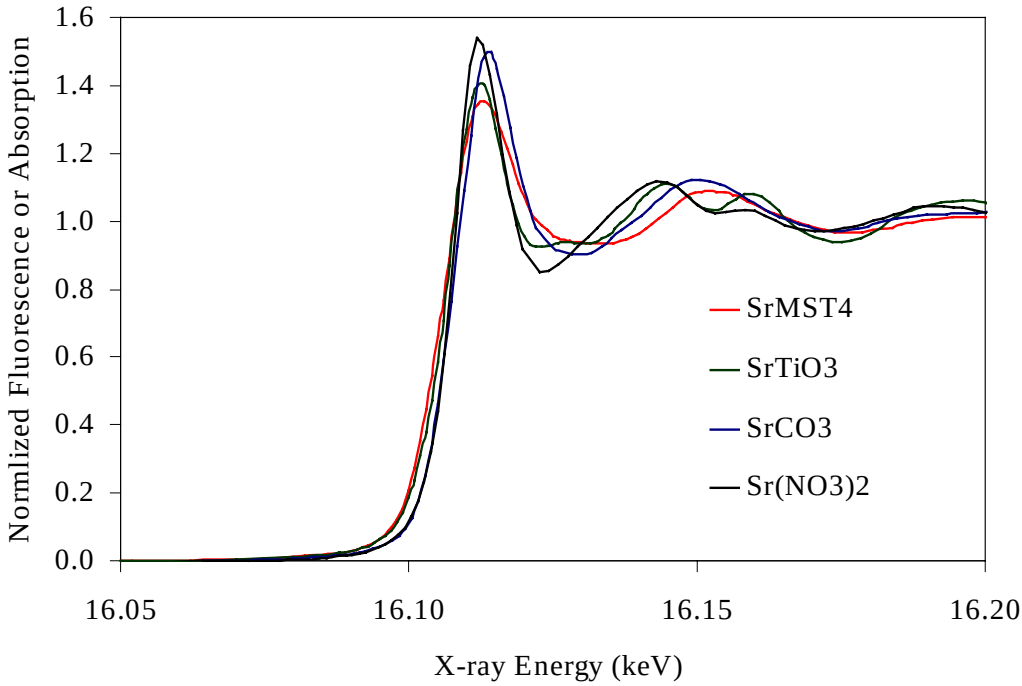

the remaining data at beamline X26a.

Figure 4-3 Plot of the Sr-XANES data for a Sr^{2+}-loaded MST sample and the Sr^{2+}-containing solids. We acquired the data for Sr standards at beamline X26a and acquired data for SrMST4 at beamline X23a2**.**

4.2 EXAFS Analyses.

In simple terms, chi data (the plot of the wavevector in reciprocal space) show the oscillation patterns (both constructive and destructive interference patterns) of the atoms in the neighbor environment of the element of interest. The chi data represent part of the photoelectron wave that can be defined by the EXAFS equation.[5,6,26] The EXAFS equation is shown in a highly simplified form below (see list of definitions for explanation of equation terms).

$$\mathrm{Chi}(k) = \frac{F(k)*N*S}{k*R^2} S_0^2 e^{(-2*k^3\sigma^2)} \sin[2*k*R + \delta(K)]$$

As noted in the methods, the XAFS data were taken at beamlines X23a2 and X26a. The location of data acquisition is noted in the figure or figure caption.

4.2.1 The k^{3-}weighted Chi Data for the Sr Standards and Sr-Loaded MST.

The k^3-weighted chi data (the EXAFS wavevector component) for the four Sr^{2+}-loaded MST treatments and the dilute Sr^{2+} in aqueous solution are shown in **Figure 4-4**. The EXAFS data for the four Sr^{2+}-loaded MST samples were very similar. The chi data indicate the environment around the Sr^{2+} sorbed on MST is unlike that of Sr^{2+} in an aqueous solution—as evidenced by the substantial difference in the amplitudes of the sample and solution data at low chi. This difference in amplitude could be indicative of unlike first-shell coordination numbers. The sample spectra also indicate that the first shell bond distance is slightly shorter than that of the Sr^{2+} in an aqueous solution. The shift in the phase indicates a shorter bond length exists for the sample spectra relative to that of the Sr^{2+} in aqueous solution. This shift is most visible in the low energy portion of the chi data (**Figure 4-4**).

The chi data for the Sr^{2+}-loaded MST samples were also unlike that of Sr^{2+} in HLW salt simulant and in $SrCO_{3(s)}$ (**Figure 4-5**). One of the differences is there are beat nodes in the spectra for the Sr^{2+} in the HLW salt solution and in $SrCO_{3(s)}$ and but they are absent in the spectra for the of Sr^{2+}-loaded MST samples (**Figure 4-4** and **Figure 4-5**). **Figure 4-6** shows the chi data for the $SrTiO_{3(s)}$ that was acquired at beamlines X23a2 and X26a. The data compare well and they indicate that the Sr^{2+} in the Sr^{2+}-loaded MST samples is not similar to that of the Sr^{2+} in the $SrTiO_{3(s)}$. This solid has a cubic structure and although the chi spectra appear to have light atoms (such as O) (as evidenced by the envelope at low chi which starts at 3 $Å^{-1}$ and disappears at around 8 $Å^{-1}$), the spectra for $SrTiO_{3(s)}$ do not resemble that of the MST samples (compare **Figure 4-4** with **Figure 4-6**). There are obvious differences in the phase and amplitude of the spectra for the MST and the $SrTiO_{3(s)}$. Data for $Sr(NO_3)_{2(s)}$ (in search of structural data) were also very different than that the Sr^{2+}-loaded MST (compare **Figure 4-4** with **Figure 4-7**).

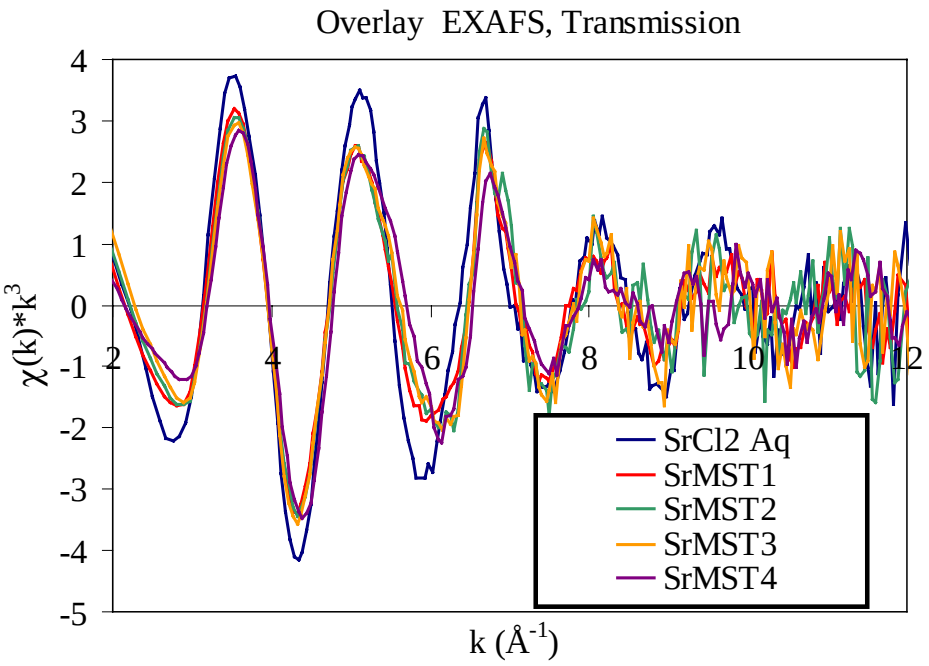

Figure 4-4 The k^3-weighted chi data (the plot of the wavevector in reciprocal space) for the Sr^{2+}-loaded MST samples. We collected the data at beamline X26A—with the exception of that for SrMST4, which we collected at X23a2.

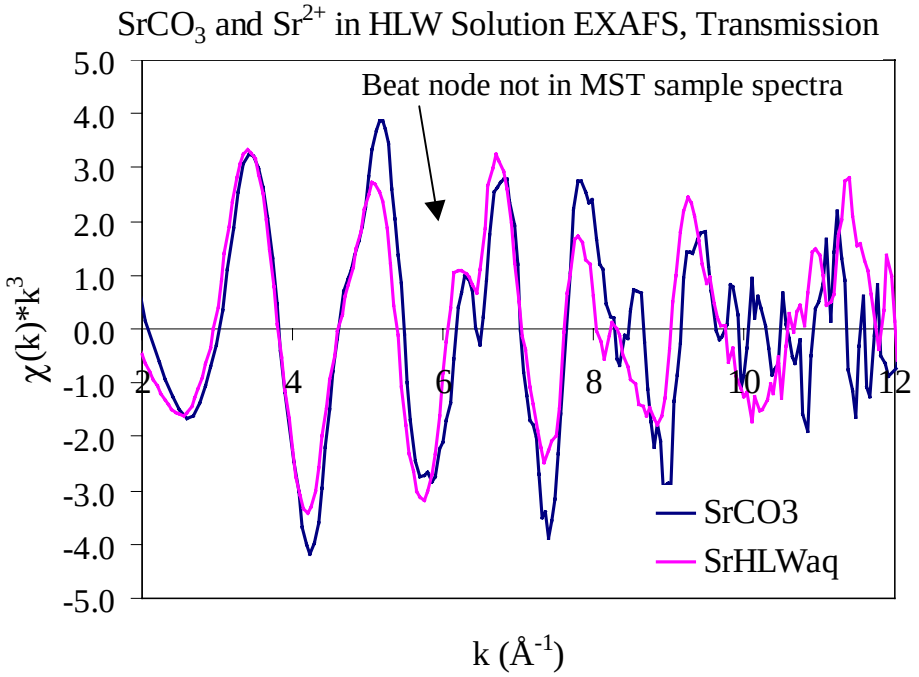

Figure 4-5 The k^3-weighted chi data for Sr^{2+} in $SrCO_{3(s)}$ and $SrHLW_{(aq)}$. We collected the data at beamline X26A.

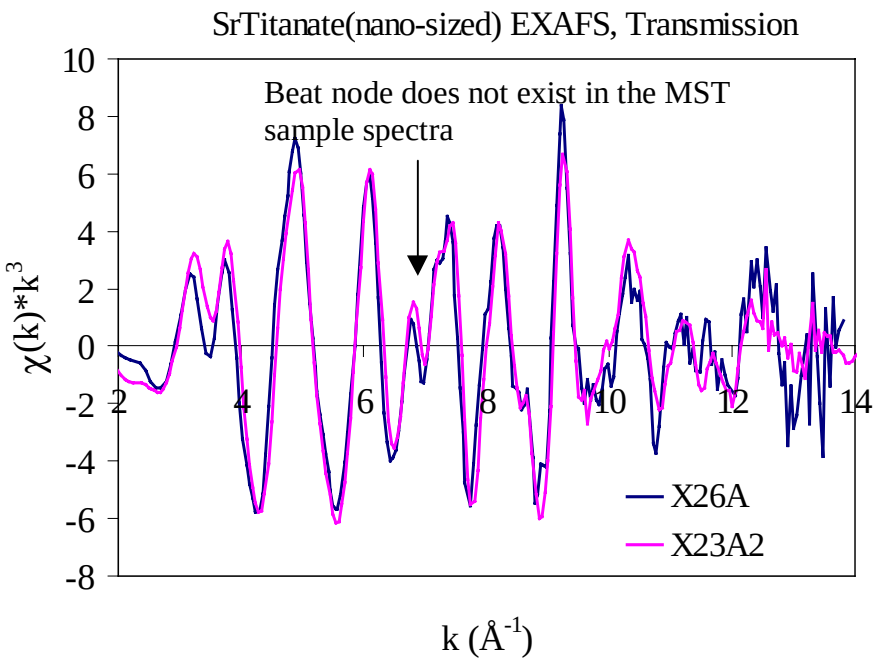

Figure 4-6 The k^3-weighted chi data for Sr^{2+} in $SrTiO_{3(s)}$. We collected the data at beamlines X26a and X23a2.

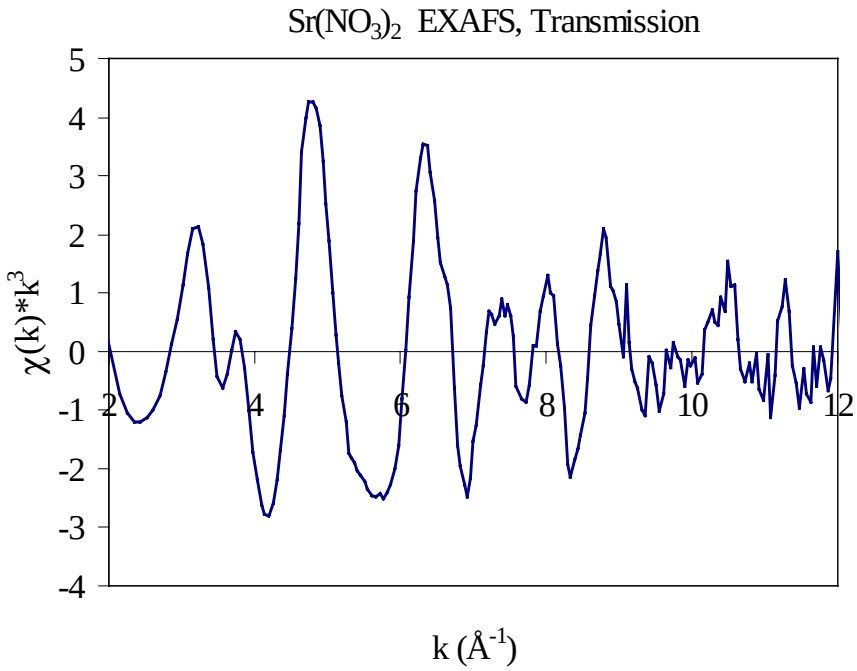

Figure 4-7 The k^3-weighted chi data Sr^{2+} in $Sr(NO_3)_{2(s)}$ We collected the data at beamline X26a.

4.2.2 Fourier-Transformed Data for the Dilute $SrCl_2$ Solution and Sr^{2+}-loaded MST.

An overlay of the Fourier-transformed (FT) radial distribution function (RDF) plots for the Sr^{2+} in dilute solution and the four Sr^{2+}-containing MST samples is shown in **Figure 4-8.** In simpler terms, these plots give radial information about the radial atom "density" around the Sr^{2+} in the sample. **Figure 4-9** shows the similarities between each of the Sr^{2+}-containing MST samples and the dilute Sr^{2+} solution. The shoulder feature on the low R side of the primary peak in the FT data could not be included in our fits of the first shell interactions in any of our data. Comparing our FT data with that of the literature, we find that this lack of fit is common to most all of the FT Sr-EXAFS data and no explanation of this shoulder feature has been provided by these references.

As discussed in **Section 4.2.1**, there were substantial differences observed between the chi spectra for Sr^{2+}-sorbed on MST and that of the Sr^{2+} in HLW solution and Sr^{2+} in the solid phase standards. Therefore, Sr^{2+} in dilute solution was deemed the best standard from which to fit the spectra of the MST samples. Model fits and transforms were only performed on the spectra for three of the four MST samples. Fits for the SrMST2 treatment were not performed due to insufficient data. The RDF distribution plots for the Sr^{2+} in dilute solution standard and three of the four Sr^{2+}-containing MST samples are shown in **Figure 4-10** through **Figure 4-15**. Two FT RDF plots are shown per Sr^{2+}-loaded MST treatment. These plots represent two mathematical approaches to the model fits. One method uses the standard EXAFS equation. The second method uses the EXAFS equation and a third cumulant (C3) term. As previously discussed the rationale for including the C3 term is discussed in the works of O'Day et al. (2000) and others.[17,18] This additional term is used to account for the anharmonicity of low atomic weight back-scatterers.[17,18]

Our analyses used the value obtained for the CN of solution Sr^{2+} (~9.5) by O'Day et al. (2000) and those values were used to obtain an amplitude reduction factor. The obtained amplitude reduction factors for both Sr^{2+} sorbed on MST and $Sr^{2+}_{(aq)}$ were fixed. This gave a CN for Sr^{2+} to O of 7 for Sr^{2+}-sorbed on MST that was considerably lower than that which we determined for $Sr^{2+}_{(aq)}$ (CN=9) (shown in **Figure 4-15** and **Table 4-3**). This decrease in the CN is significant—indicating that Sr^{2+} undergoes dehydration upon sorption to MST.

However, when the third cumulant term (C3) is included in our data analyses, the first shell CN for Sr^{2+} decreased from about 7 to 10 to about 5 to 7. Without the use of the third cumulant term, the fitting analyses of the Sr-EXAFS data for Sr^{2+} in solution indicate the first shell environment for Sr^{2+} contains roughly 9.5 first shell O atoms at 2.57 Å (**Table 4-2**). Similar results were obtained when we used the third cumulant in our analyses. Our findings contrast with that in other studies.[18] O'Day et al. (2000) found that adding the C3 term produced a better fit for solution Sr^{2+} whereas we did not observed a better fit with the C3 term for aqueous Sr^{2+}. In conclusion, fits with the C3 term were substantially better than that without the term. When the C3 term was included, the magnitude of the Debye-Waller Factor values were lower and the fits were visually better as seen by comparing **Fig, 4-10** with **Fig, 4-11, Fig. 4-12** with **Fig. 4-13** and **Fig. 4-14** with **Fig. 4-15**.

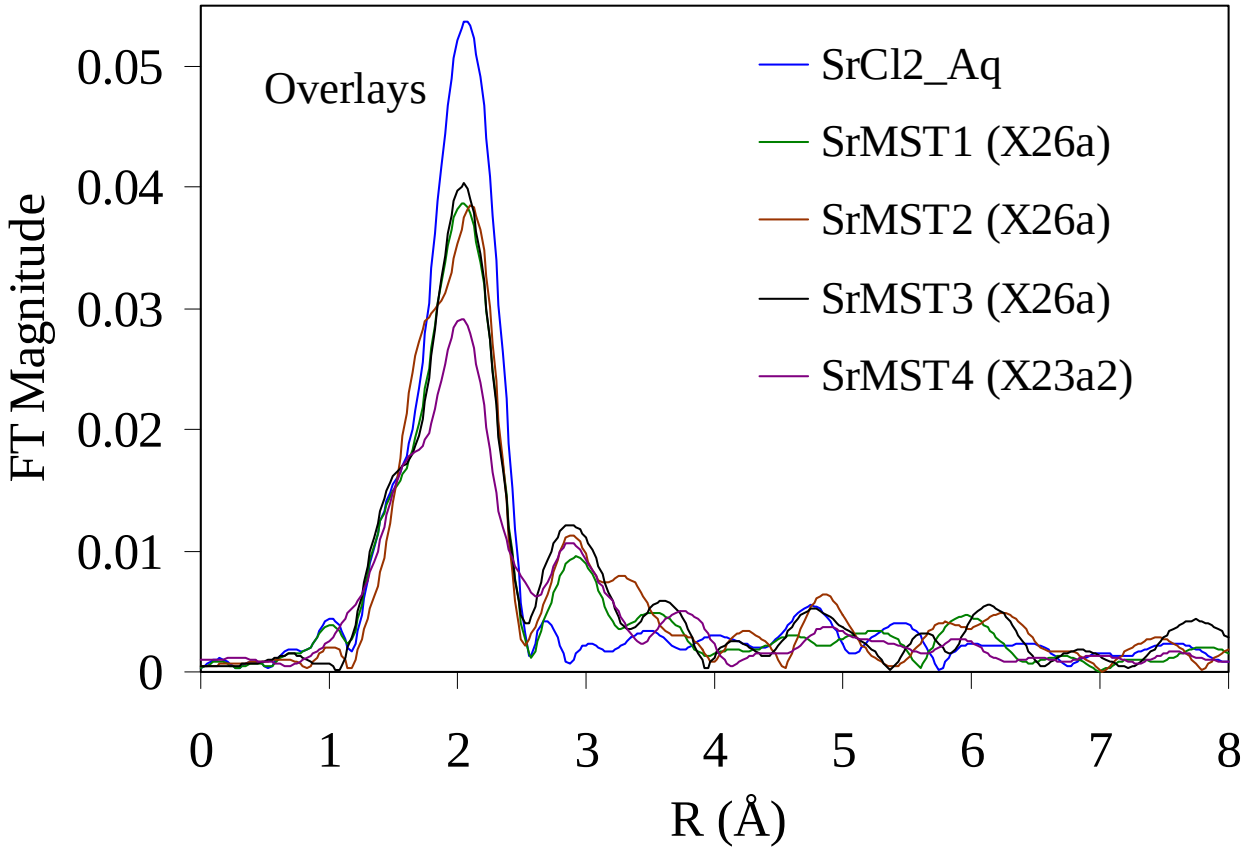

Figure 4-8 FT RDF data for Sr^{2+}-loaded MST samples and the $SrCl_{2(aq)}$ standard.

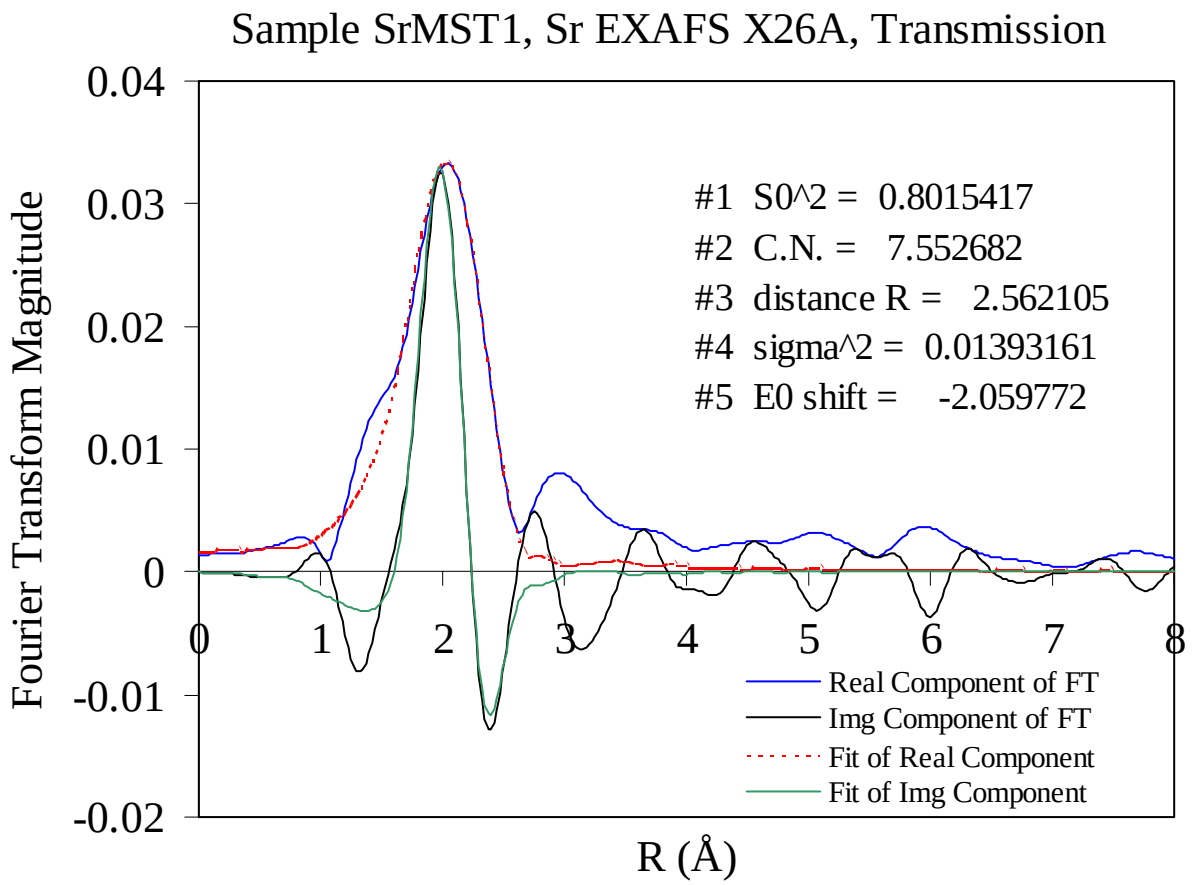

Figure 4-9 FT RDF data and first shell Sr-O model fit data for SrMST1 without the third cumulant term—uncorrected for phase shift.

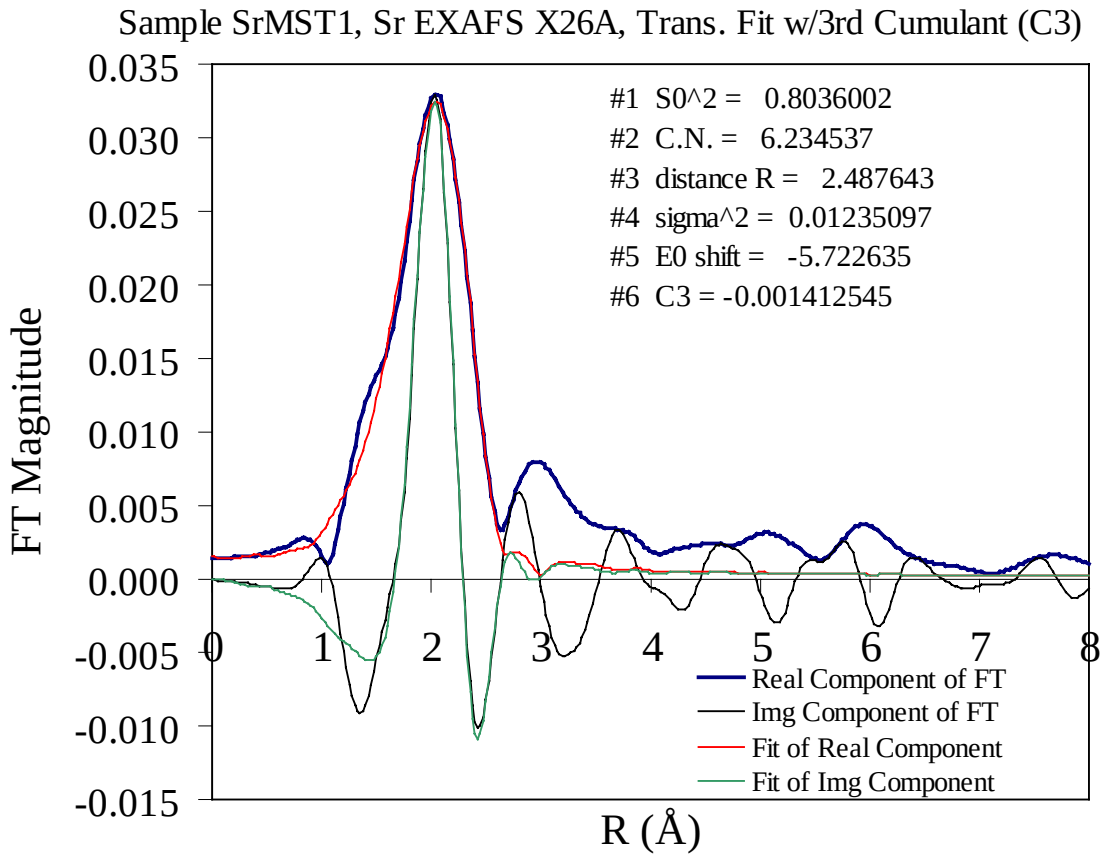

Figure 4-10 FT RDF data and first shell Sr-O model fit data for SrMST1. The third cumulant term was included in the fit—uncorrected for phase shift.

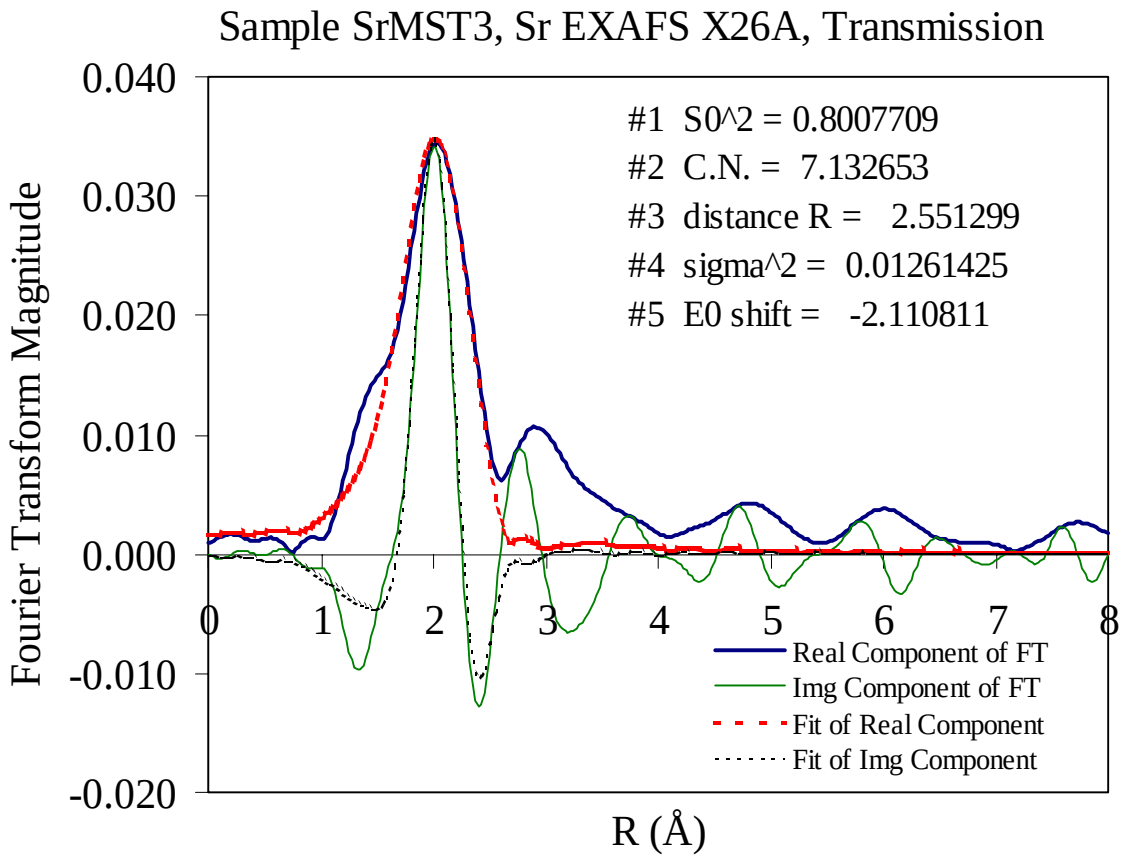

Figure 4-11 FT RDF data and first shell Sr-O model fit data for SrMST3 without the third cumulant term—uncorrected for phase shift.

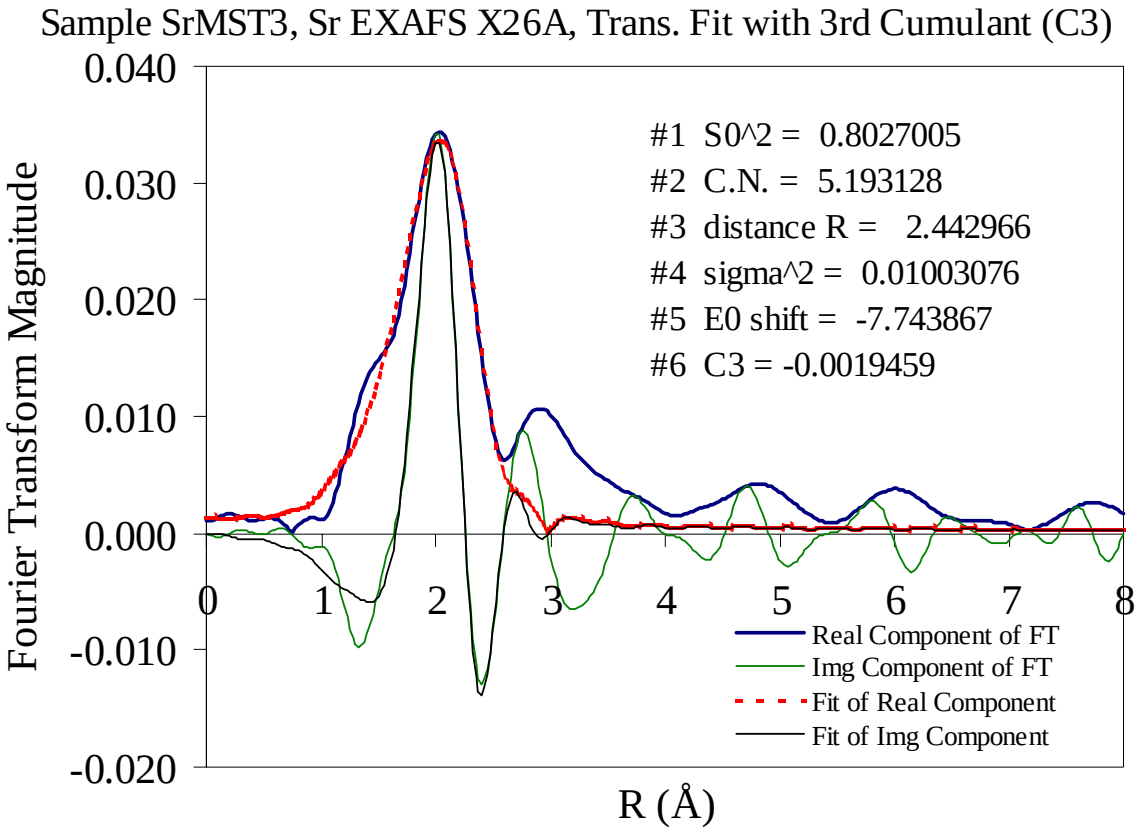

Figure 4-12 FT RDF data and first shell Sr-O model fit data for SrMST3. The third cumulant term was included in the fit—uncorrected for phase shift.

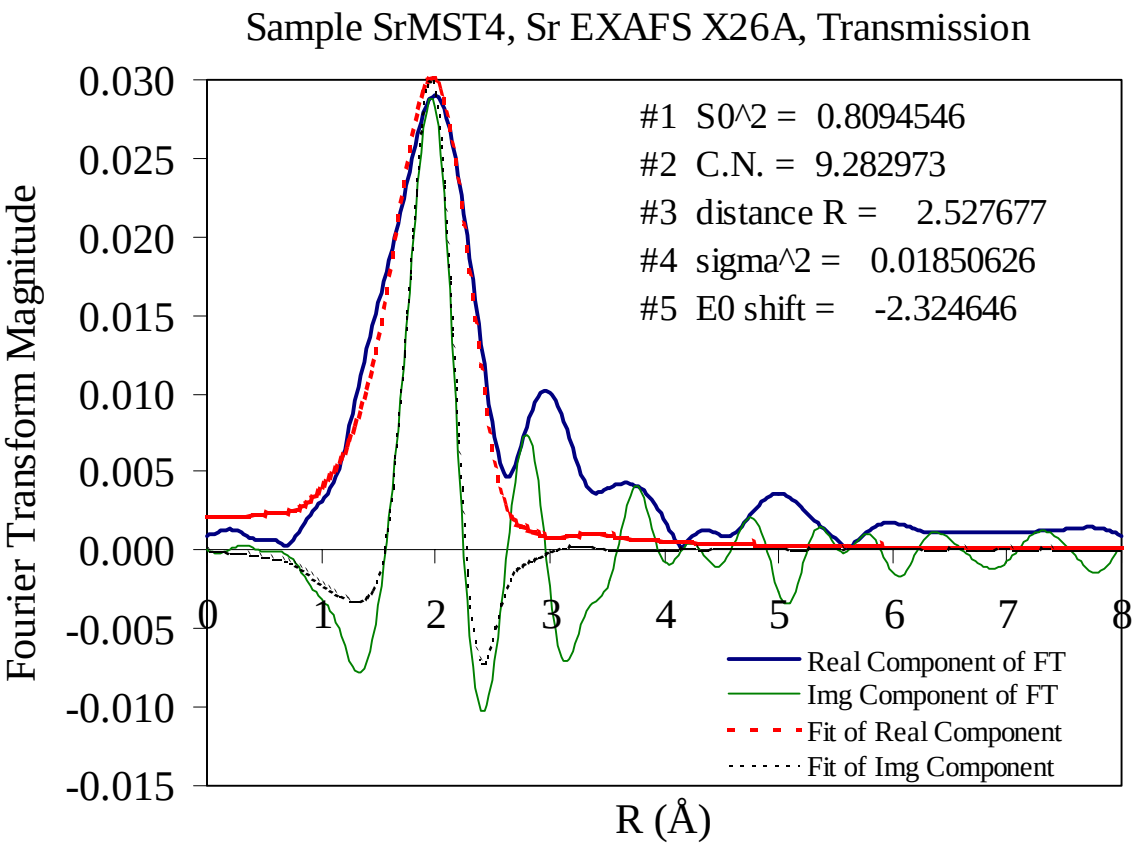

Figure 4-13 FT RDF data and first shell Sr-O model fit data for SrMST4 without the third cumulant term—uncorrected for phase shift.

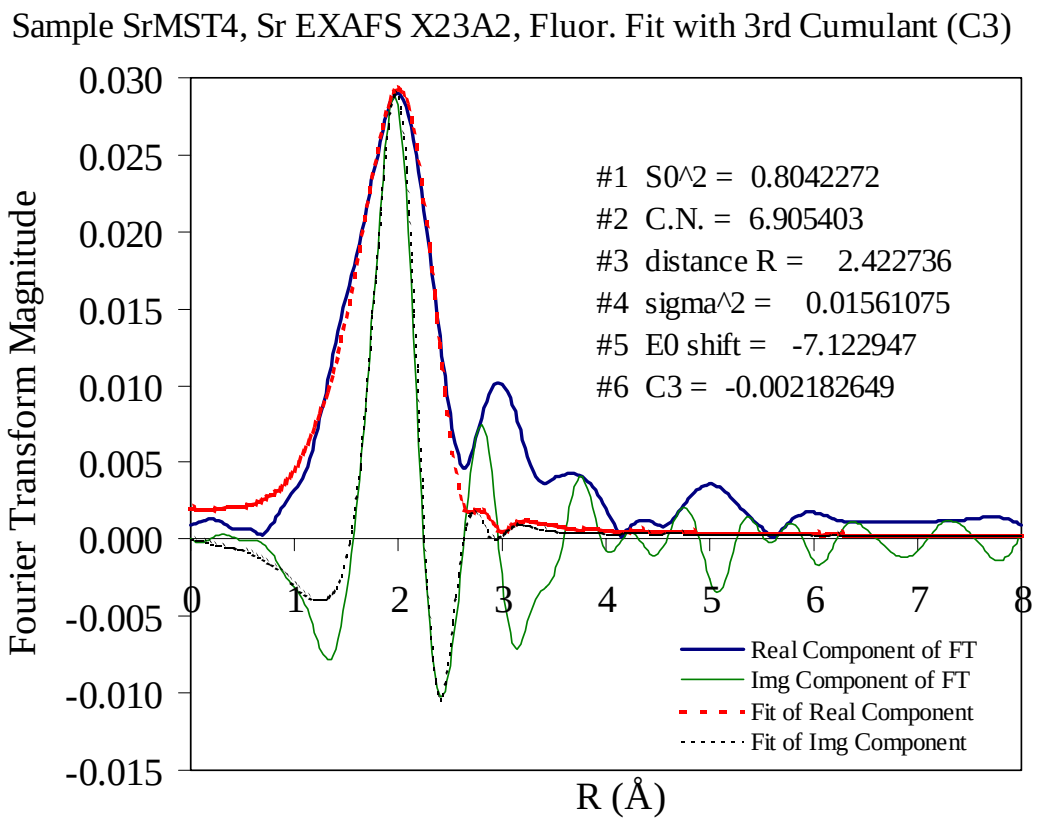

Figure 4-14 FT RDF data and first shell Sr-O model fit data for SrMST4. The third cumulant term was included in the fit—uncorrected for phase shift.

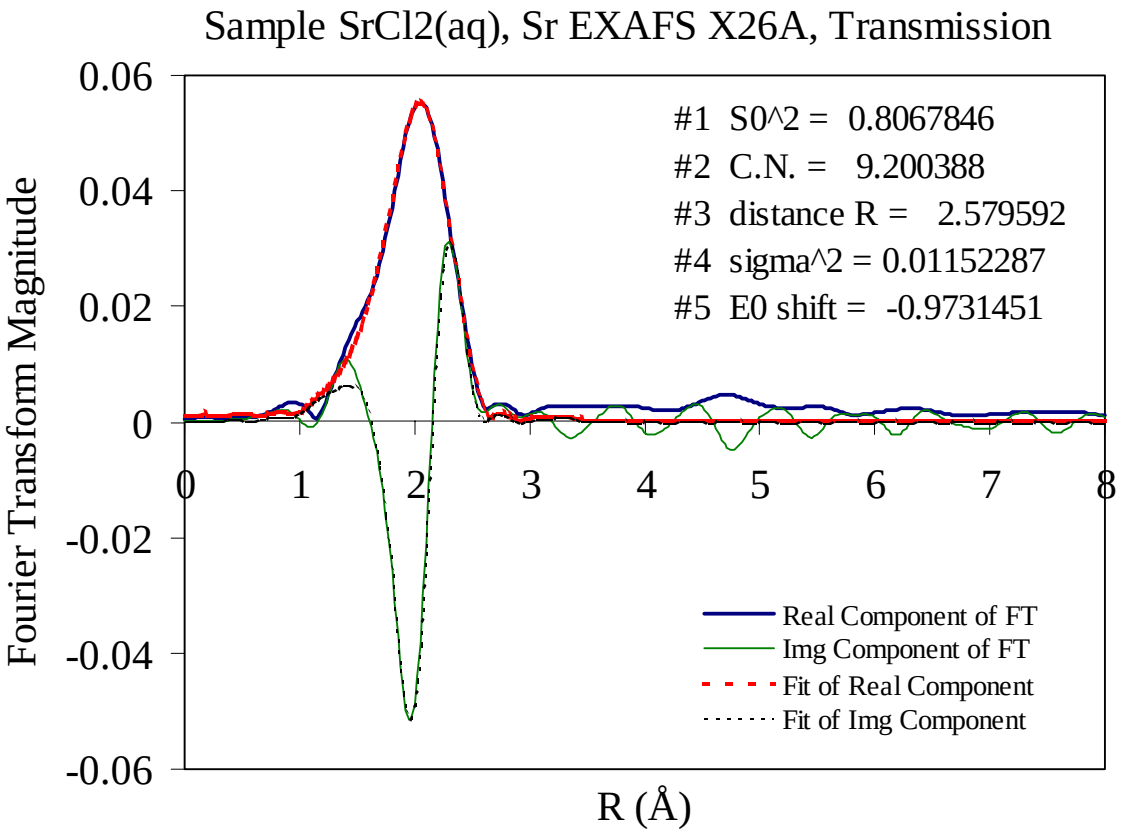

Figure 4-15 FT RDF data and first shell Sr-O model fit data for the dilute $SrCl_2$ solution without the third cumulant term—uncorrected for phase shift.

Table 4-3 Fit results for a first shell Sr-O interaction with and without the third cumulant (C3) term for the Sr^{2+} sorbed MST samples. Use of the third cumulant term in the fits for Sr in the dilute $SrCl_{2(aq)}$ solution yielded no differences (in CN or R). Fits for SrMST2 were not performed due to insufficient data quality. DeltaR and deltaCN represent the change in R and CN values (respectively) with the inclusion of the C3 term. The magnitude of the Debye-Waller Factor [represented in as $\sigma^2[Å]^2$] indicates the variation of the bond length determination (or spread but not error). It also provides information on goodness of fit—for example, a negative value would indicate a poor fit. A decrease in the D-W factor with inclusion of the C3 term signifies that there is less variance and hence better fit. Addition of the third cumulant (C3) term in the fit accounts for the anharmonicity arising from weak back-scatterers. The addition of this C3 variable in the fitting process should result in a smaller D-W factor. Without the C3 term, the D-W factor is overestimated.

	Interaction	**CN**	**R(Å)**	**$\sigma^2[Å]^2$**	**deltaR**	**deltaCN**
$SrCl_{2(aq)}$	Sr-O	9.5	2.57	0.0115	NA	NA
SrMST1	Sr-O	7.6	2.55	0.0139	0.6	1.4
SrMST1 + C3	Sr-O	6.2	2.49	0.0123		
SrMST2	Sr-O	No Fits	No Fits	No Fits	No Fits	No Fits
SrMST2 + C3	Sr-O	No Fits	No Fits	No Fits	No Fits	No Fits
SrMST3	Sr-O	7.1	2.55	0.0126	0.11	1.9
SrMST3 + C3	Sr-O	5.2	2.44	0.010		
SrMST4	Sr-O	9.3	2.53	0.0185	0.11	2.4
SrMST4 + C3	Sr-O	6.9	2.42	0.0156		

The magnitude of the Debye-Waller Factor [represented in as $\sigma^2[Å]^2$] indicates the variation of the bond length determination (or spread but not error). It also provides information on goodness of fit—for example, a negative value would indicate a poor fit. A decrease in the D-W factor with inclusion of the C3 term signifies that there is less variance and hence better fit.

4.2.2.1 Higher Shell Fits for Sr-Ti and Sr-O Interactions.

The fits were performed in chi space because this provided better separation of the atoms in the higher shells. The higher shell fitting process began with sample SrMST1 by fitting for a second shell Sr-O interaction with and without the third cumulant term (fit results shown in **Table 4.4**) but these fits were not adequate. Most of the attempted fits (shown in the **APPENDIX**) for SrMST1 were unsatisfactory—as shown in **Figures 8-1** through **8-7** and discussed below. [Note: the figures show back-transformed (Fourier-filtered) higher shell data that do not contain the first shell Sr-O interactions.]

Fits that included a second shell Sr-Ti interaction with and without the C3 term and these fits were not satisfactory. Third shell fits for a Sr-O interaction were attempted with and without the C3 term and these fits were not satisfactory. Third shell fits with a Sr-Ti interaction did not converge. A combination of a single second shell Sr-Ti interaction and a third shell Sr-O interaction were better at describing the data but the most successful fits were obtained by fitting two second shell Sr-Ti interactions and a third shell Sr-O interaction—as shown in **Figure 4-16**. For the SrMST1 sample, our attempts to fit first shell Sr-Sr interactions were not successful (i.e., they did not converge).

The EXAFS data for the MST samples were so similar, fits were only performed for the SrMST3 and SrMST4 data using two second shell Sr-Ti interactions and a single third shell Sr-O interaction (fits shown in **Figures 4-17** and **4-18**). Model fits for Ti in the second shell of the Sr^{2+} for the remaining SrMST samples produced similar results (SrMST1, SrMST3 and SrMST4 as shown in **Table 4-4**). Fits for Ti in the second coordination shell for Sr^{2+} (**Table 4-4**) typically indicate the presence of two or more Ti atoms between 3.42 Å and 3.63 Å—suggesting more than one TiO_6 octahedron (**Figure 4-17**) is present in the local environment. The radial distances of higher shell O atoms ranged from 3.9 to 4.01 Å.

There is considerable spread in the third shell CN values for the Sr-O interactions in the three SrMST samples (**Table 4-4**). Although we obtained CN values from our third shell fits, they are in general, not as reliable as first shell and second shell CN values. This is because information obtained at higher radial distances from the absorbing atom is more subject to noise and the signal is weak—particularly for a light atom such as O. The CN values are related to the amplitude of the EXAFS oscillations. In contrast, the atomic distances in EXAFS spectra are related to the frequency of the oscillations, which is less subject to noise and atom weight than that of CN values. Another factor that could introduce some error in our CN value determinations is that we did not account for multiple scattering paths. Accounting for multiple scattering paths (in addition to single scattering paths) is not straightforward when the structural arrangement of the atoms is not known. We did not know the structure of local environment of these atoms so multiple scattering paths were not included. Hence, third shell fit data for sorbed Sr^{2+} species are typically, absent in the literature.

4.3 Modeling of Sr^{2+} Sorption on MST

Based on model fits of the EXAFS data, molecular models were generated using the program Chem3D.[27] The modeling assums the Ti are octrahedrally coordinate to O as would be consistent for an amorphous form of Sr^{2+} nonatitanate.[28] Arrangement of a Sr^{2+} atom bound to a single TiO_6 octahedron is shown in **Figure 4-21** and an arrangement of a Sr^{2+} bound to a four TiO_6 octahedron is shown in **Figure 4-23**. Although the structure of MST is not known, these models suggest that Sr^{2+} is associated with the MST via a specific adsorption mechanism because the distance between the Sr^{2+} and the Ti is short enough and the models support this conclusion. Some structural incorporation cannot be excluded but the low amount of Ti (two atoms on average) in the second coordination shell of the Sr^{2+} suggests that specific adsorption to the MST surface is the dominant mechanism of metal uptake of Sr^{2+}.

Table 4-4 Fit results for a second and third shell Sr interactions with and without the third cumulant (C3) term for the Sr^{2+} sorbed MST samples. Use of the third cumulant term in the fits for Sr in the dilute $SrCl_{2(aq)}$ solution yielded no differences (in CN or R). The third cumulant term was not included in fits for second and third shell interactions due to a limited number of degree of freedom, which did not allow addition of another floating variable. Fits for SrMST2 were not performed due to insufficient data quality.

Sample	Shell	Interaction	CN	R(Å)	σ^2[Å]^2
SrMST1	Second	Sr-O	6.22	3.87	0.02
		Sr-O with C3	5.70	4.02	0.01
		Sr-Ti	3.64	3.52	0.025
		Sr-Ti with C3	2.77	3.59	0.02
	Third	Sr-O	1.20	3.98	0.0029
		Sr-O with C3	1.29	4.03	0.0029
		Sr-Ti or Sr-Sr	ND	fit did not converge	ND
	Second and Third	Sr-Ti Sr-O	0.70 2.15	3.46 3.92	0.008 0.006
		$Sr\text{-}Ti_1$ $Sr\text{-}Ti_2$ $Sr\text{-}O_1$	1.10 0.65 2.20	3.42 3.51 3.91	0.002 0.001 0.005
SrMST2	Second and Third	$Sr\text{-}Ti_1$ $Sr\text{-}Ti_2$ $Sr\text{-}O_1$	No Fits No Fits No Fits	No Fits No Fits No Fits	No Fits No Fits No Fits
SrMST3	Second and Third	$Sr\text{-}Ti_1$ $Sr\text{-}Ti_2$ $Sr\text{-}O_1$	2.40 2.80 7.05	3.43 3.52 3.90	0.0014 0.0003 0.0079
SrMST4	Second and Third	$Sr\text{-}Ti_1$ $Sr\text{-}Ti_2$ $Sr\text{-}O_1$	1.39 1.15 1.75	3.53 3.63 4.01	0.0015 0.0003 0.0048

4.4 Comparison of First Shell Coordination Data with Literature Findings

Our findings for the first shell interactions of Sr^{2+} and O are most similar to that of Sr^{2+} in heulandite, and of Sr^{2+}-sorbed on kaolinite, silica and FeOOH (goethite).[18,19,23] O'Day et al. (2000) did not use the C3 term in their fits for Sr^{2+} in the zeolite (P. O'Day, Univ. of Arizona, personal communication, 2001). Sahai et al (2000) and Parkman et al. (1998) did not use the C3 term in their fits.[18,19] However, our data without the C3 term are similar (compare **Table 4-1 and Table 4-3**). The Sr-EXAFS data for heulandite have a Sr-O interaction with a CN value of 8 and a Sr-O distance of 2.60 Å, which compares well with our data analyses that did not used the C3 term (**Tables 4-1 and 4-3**).[18] Collins et al. (1998) did not use the C3 term in their fits however, their work with Sr^{2+}-sorbed FeOOH in pH 10.2 solutions show 8 first shell O atoms at 2.6 Å and these results compare well with ours.[23] Our Sr-EXAFS data do not compare as well with the other first shell data in the literature for sorbed Sr^{2+} species listed in **Table 4-1**.

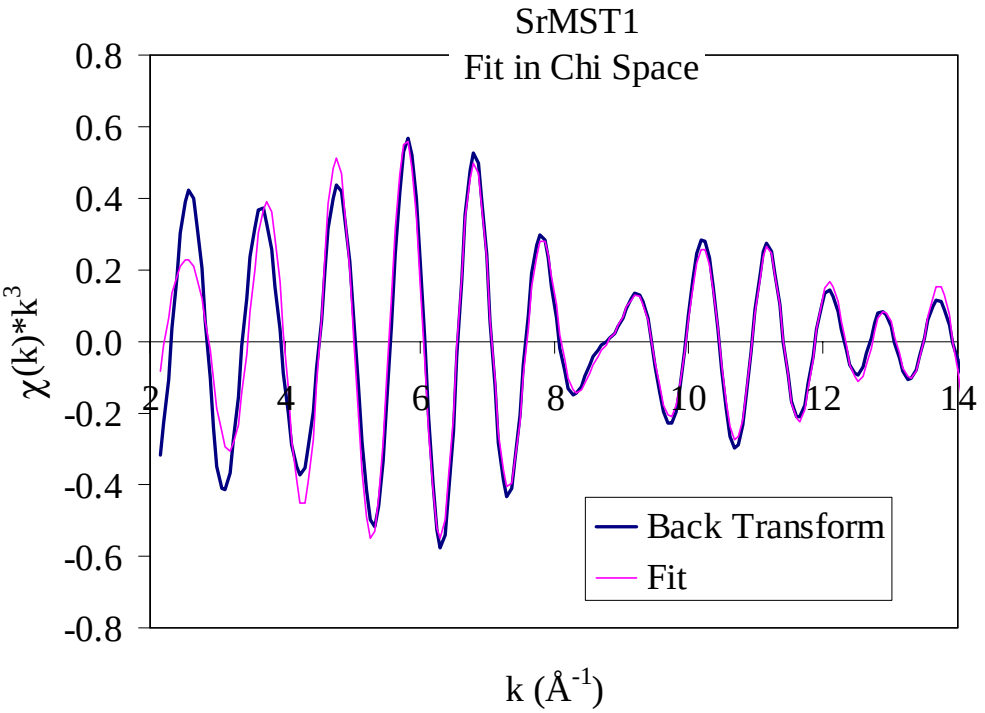

Figure 4-16 Back-transformed chi data and model second and third shell fit data for interactions of Sr-Ti_1, Sr-O_1 and Sr-Ti_2 for Sr^{2+}-loaded SrMST1.

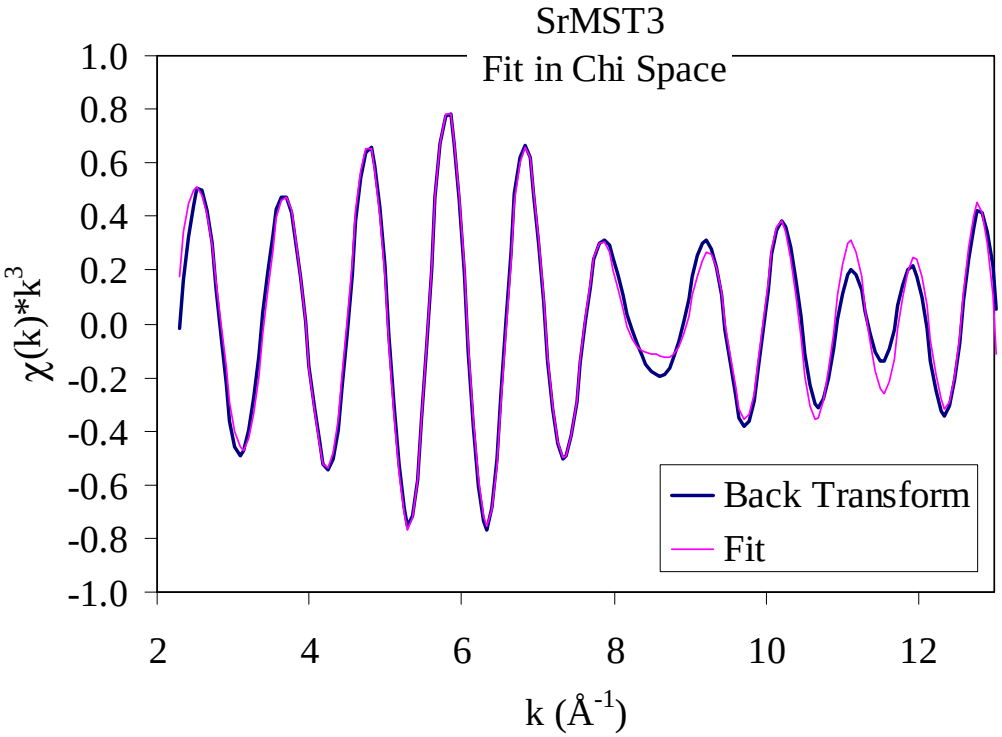

Figure 4-17 Back-transformed chi data and model second and third shell fit data for interactions of Sr-Ti_1, Sr-O_1 and Sr-Ti_2 for Sr^{2+}-loaded SrMST3.

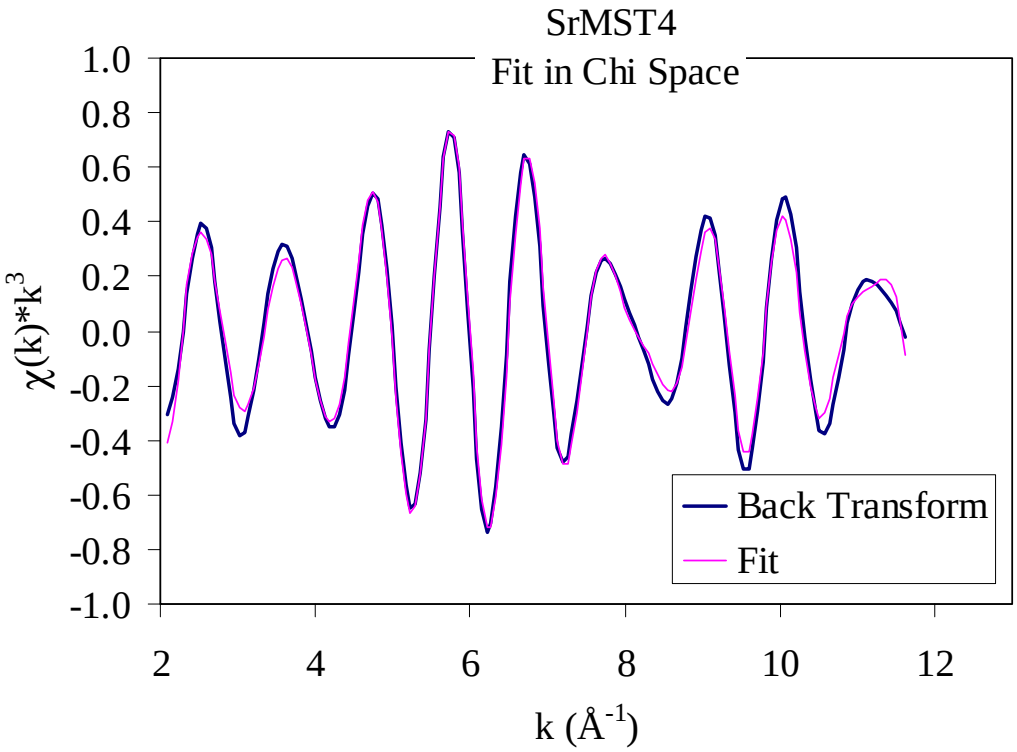

Figure 4-18 Back-transformed chi data and model second and third shell fit data for interactions of Sr-Ti_1, Sr-O_1 and Sr-Ti_2 for Sr^{2+}-loaded SrMST4.

4.5 Comparison of Second and Third Shell Coordination Data with Literature Findings

Our findings for the second shell interactions of Sr^{2+} and Ti are most similar to that of Sr^{2+} in heulandite, which had two second shell Si/Al radial distances with CN values of 2 at 3.49 and 4.14 Å.[18] No other Sr-EXAFS studies have reported the existence two second shell atoms at two different distances around the Sr^{2+} (**Table 4-1**). However, such fits require high quality data acquisition, which is difficult when light atom back scatterers are present in the spectra.

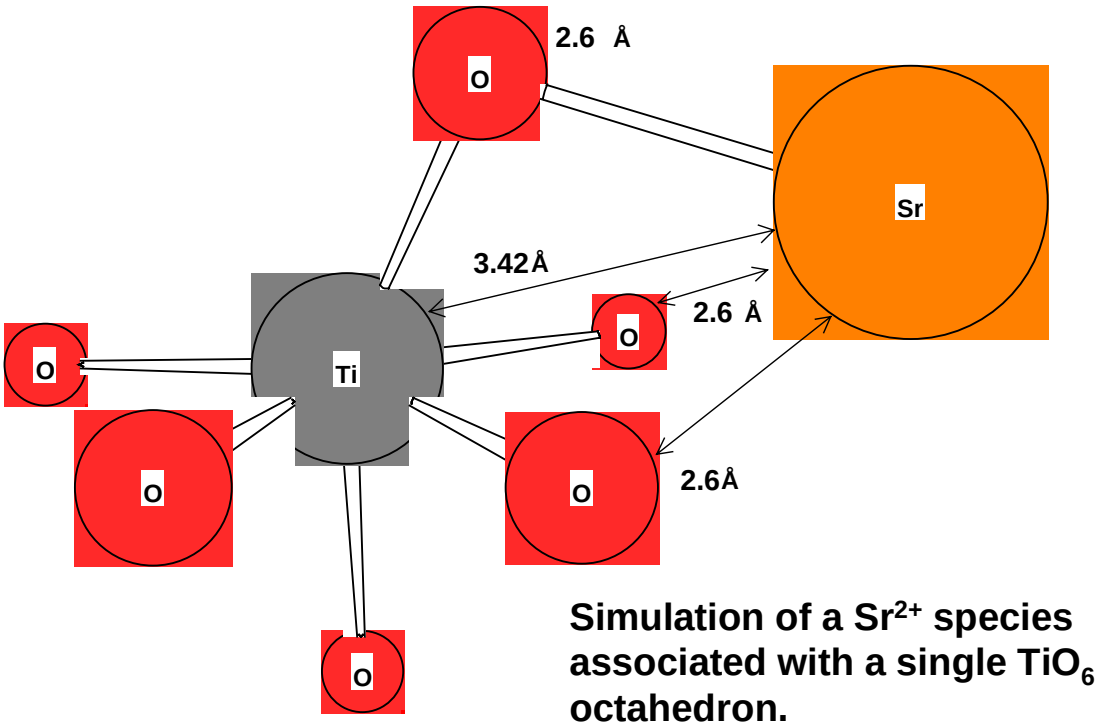

Figure 4-19 EXAFS-based molecular model of association of Sr^{2+} with TiO_6 groups.

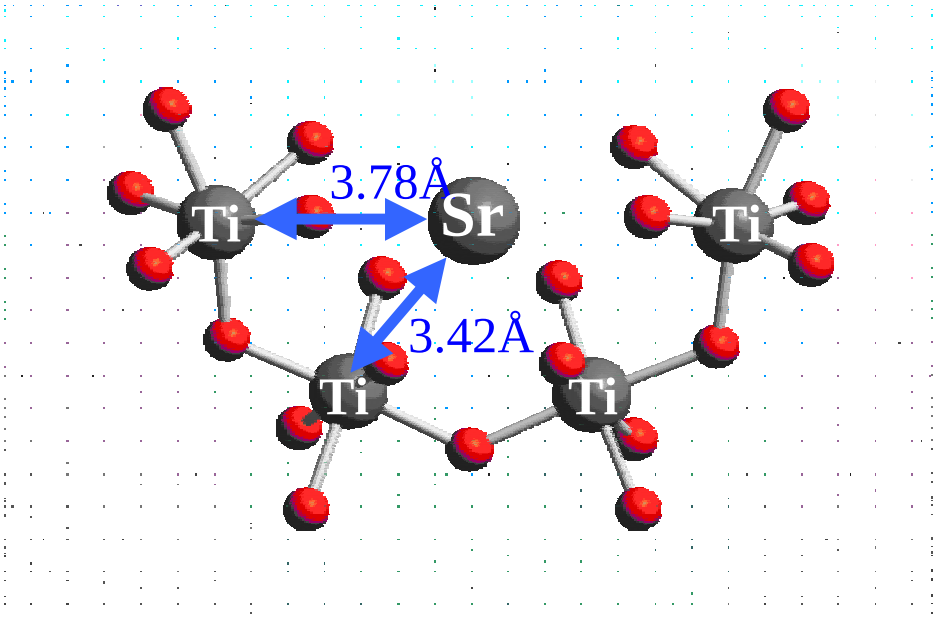

Figure 4-20 EXAFS-based molecular model of association of Sr^{2+} with corner-shared TiO_6 groups.

5.0 DISCUSSION AND CONCLUSIONS

5.1 Determination of the Uptake Mechanism.

Strontium sorption studies were conducted using MST and XAFS data collection was conducted on these materials and reference solid and aqueous materials. The literature on Sr^{2+} sorption was reviewed and compared with the results of our studies. Data analyses were performed on the Sr-XAFS data for the MST samples and on one of the Sr^{2+} references. The XANES and EXAFS data indicate that (on average) the environments of the Sr^{2+} in the MST samples were similar and that they resembled that of solution Sr^{2+}. First and second shell fits of the Sr-EXAFS data indicate that O is in the first and third coordination shell and more than one Ti (on average) is in the second shell. The EXAFS data and the molecular modeling suggest the Sr^{2+} is closely associated with MST.

We compared our findings with Sr-XAFS studies in the literature that examined the Sr^{2+} sorption on a variety of materials. We found some similarities with the findings from the literature. However, most of these studies were conducted under environmentally relevant conditions (such as the groundwater environments under leaky HLW tanks at Hanford, WA or potentially contaminated environments at proposed nuclear waste geologic repositories). These conditions are not equivalent to that of highly alkaline HLW salt solutions. Because little is known about the local environment of sorbed Sr^{2+} species in HLW salt solutions, the literature provides a useful foundation on Sr^{2+} sorption behavior to metal oxides and methods of Sr-XAFS data analyses.

We conclude that the nature of the Sr^{2+} sorption does not involve ion exchange of fully hydrated Sr^{2+} species because there was a pronounced loss in waters of hydration upon sorption—regardless of whether the C3 term was used in the fits or not. Removal of Sr^{2+} is via specific adsorption of a partially hydrated Sr^{2+} species, which signifies that the removal mechanism is not surface precipitation—even at high Sr-loadings. The primary uptake mechanism of the Sr^{2+} is not structural incorporation. If the Sr^{2+} were present within the MST structure, it would have multiple second shell Ti atoms. For example, this is the case for Sr^{2+} in $SrTiO_3$ solid shown in **Table 4-1,** which has 6 Ti atoms in the second shell environment. The fact that only one Ti atom is present in the first shell suggests that structural incorporation is not likely and that the Sr^{2+} is bound via specific adsorption to the MST surface.

5.2 Influence of Sorption Mechanism on Process

Specific adsorption implies some good process attributes. If irreversible, this mechanism has the benefit that the Sr^{2+} will remain bound at higher temperatures and will not leach into solution and potentially transfer with the supernatant to the undesired process stream. If removal of solution Sr^{2+} occurred via surface precipitation on MST, washing of the Sr^{2+}-loaded MST would dissolve the Sr^{2+} solid phases that formed and complicate the decontamination process by partitioning the Sr^{2+} into a wash process stream. Similarly, we do not observe Sr^{2+} uptake via an outer-sphere (ion exchange), which means that the washing of the MST post decontamination would not effect the ability of the MST to retain the Sr^{2+}.

5.3 The Structure of MST is Unknown

The structure of MST is not known. High-resolution TEM and Ti-XAFS studies are likely to provide structural information that conventional X-ray diffraction techniques cannot (the MST is does not have long range order and is amorphous). It has been suggested by A. Clearfield (Texas A and M University, College Station, TX, 2001) that MST may exist as long sheet-like layers of edge-linked Ti octahedra such as in the simplified diagram below:

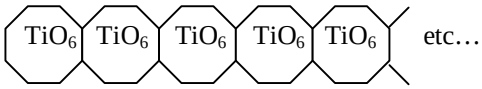

If the structure of MST contained sheets of Ti octahedra, the Sr-EXAFS information that would be obtained for the local environment of structural Sr^{2+} would be nearly equivalent to that of Sr-EXAFS information obtained for specifically adsorbed Sr^{2+}. The uptake mechanism would involve direct bonds and no outer sphere sorption or surface precipitation.

5.4 Suggestions for Further Study

Our findings are consistent with that of specific or inner sphere adsorption and they involve a partially hydrated Sr^{2+} species that binds to the MST surface. Even though specific adsorption is operative, some items in need further study. The effect of temperature on the environment of (partially-hydrated) Sr^{2+} species on surfaces has been investigated.[29] In kinetic studies, Hobbs and co-researchers observe decreased uptake of Sr^{2+} (at equilibrium) at 45 °C (relative to studies at 25 °C).[29] However, these studies were conducted with solutions of Sr^{2+} and multiple actinides. Competitive effects among the dissolved species may have been operative. At higher temperatures (65 °C) the effect of temperature on Sr^{2+} sorption is not clearly evident from the data. An increase in temperature could cause the release of waters of hydration from the sorbed Sr^{2+} species and possibly change the mechanism or amount of Sr^{2+} uptake.[29]

Another condition that could influence the sorption of dissolved species is that of competition and competition for surface sites by the Sr^{2+} and the actinides on the MST may be a function of temperature. Studies should be conducted to examine whether there is competition between Sr^{2+} with Na^{+} for sorption sites on the MST. Work has shown that decreased Sr^{2+} sorption is observed at higher Na^{+} solution concentrations (4.5 M versus 7.5 M Na^{+}).[30] Competitive sorption studies could also be done with Sr^{2+} and actinides. There could be more than one type of binding site for Sr^{2+} on the MST. Our Sr-XAFS data gives average information and we must be aware that multiple binding sites could exist on the MST. The availability of strong binding sites may decrease as they are removed from the general pool upon Sr^{2+} adsorption. This may leave weaker binding sites for other species such as the actinides.

The authors also propose a series of studies with Sr^{2+} and two other materials: SrTreat and sodium nonatitanate ($Na_4Ti_9O_{24}$) for the later portion of FY-01. Such a study will

provide fundamental insights on how sorption efficiency varies with structural features of the titanates thus guiding changes in synthesis methods to improve process performance.

On going work in this project concerns the XAFS data analyses of the U(VI) studies, and planned XAFS analyses for a suite of Np and Pu loaded MST samples. A report will be put forth on each of the actinides.

6.0 ACKNOWLEDGMENTS

The authors thank J. Woicik (NIST), A. Ackerman (BNL), W. Rao (University of Georgia), W. Tamosaitis (SRTC) and J.U. Coughlin (WSRC), for their assistance, support and bright ideas. N. Gregory, M. Bloom, and H. L. Thacker (all of SRTC) are acknowledged for their assistance in the preparation of the MST samples.

7.0 APPENDIX

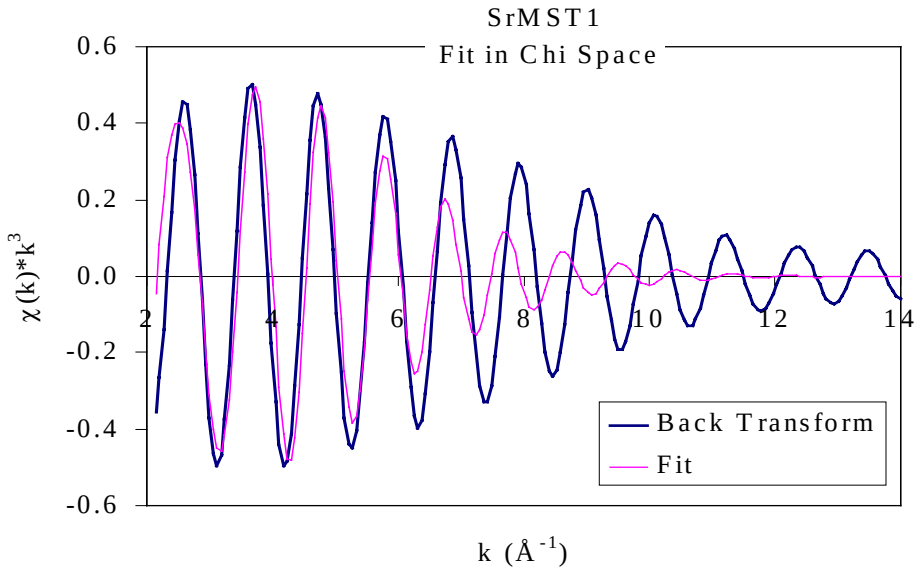

Figure 7-1 Back-transformed chi data and model fit second shell data for interactions of Sr-O without the C3 term for Sr^{2+}-loaded SrMST1.

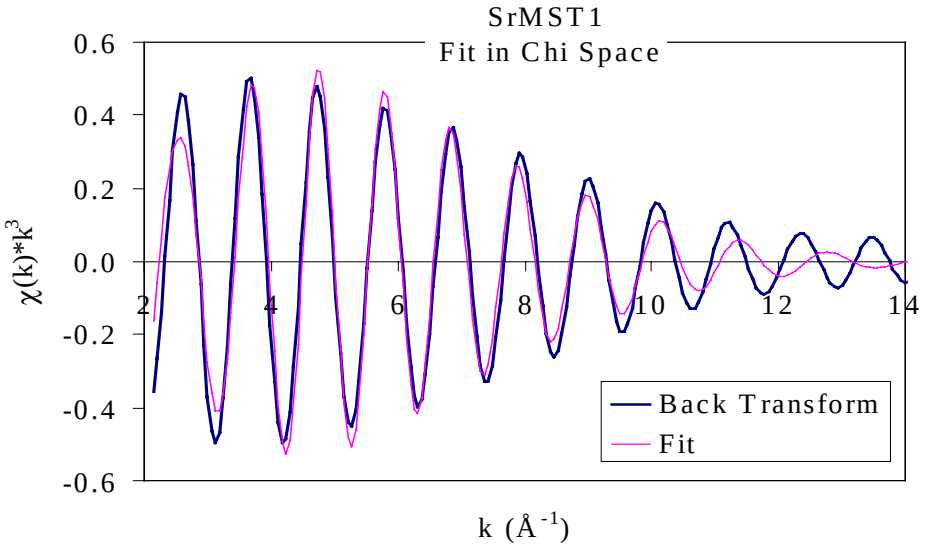

Figure 7-2 Back-transformed chi data and model fit second shell data for interactions of Sr-O with the C3 term for Sr^{2+}-loaded SrMST1.

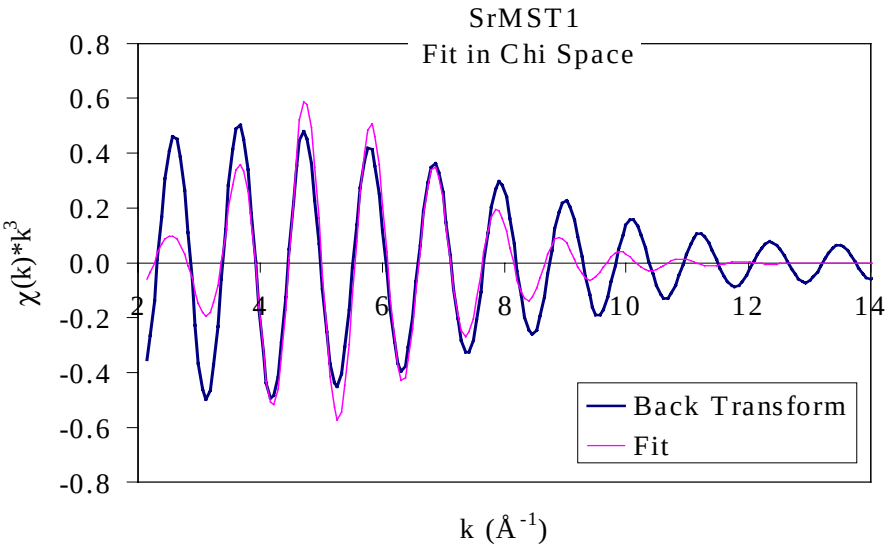

Figure 7-3 Back-transformed chi data chi data and model fit data for second shell interaction of Sr-Ti without the C3 term for Sr^{2+}-loaded SrMST1.

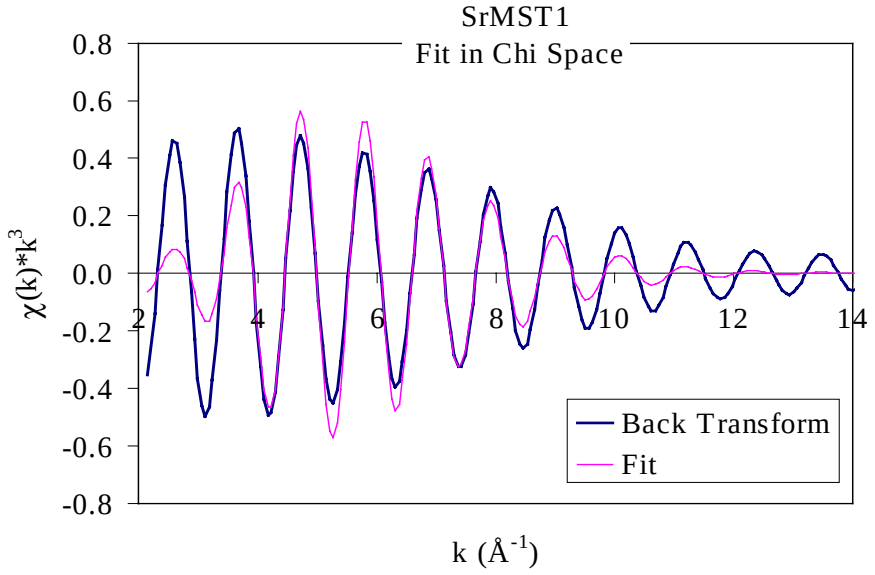

Figure 7-4 Back-transformed chi data and model fit data for second shell interactions of Sr-Ti with the C3 term for Sr^{2+}-loaded SrMST1.

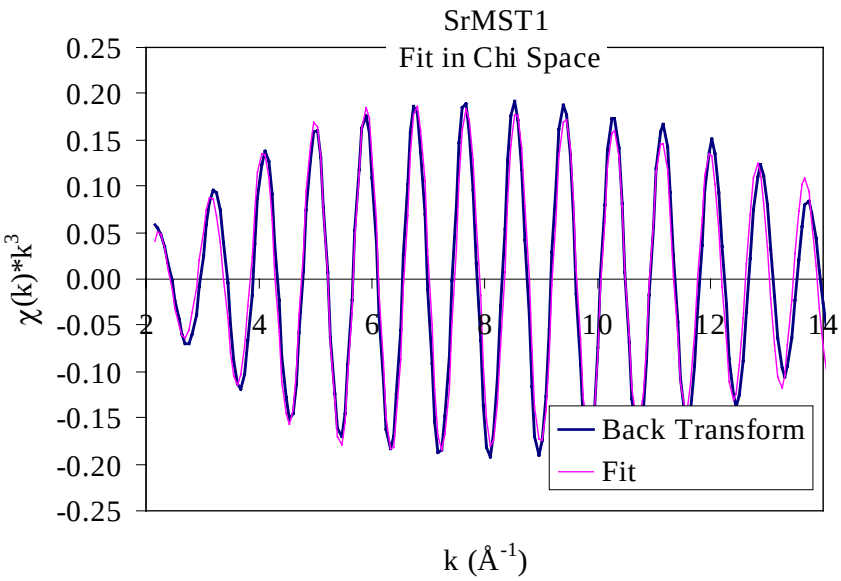

Figure 7-5 Back-transformed chi data and model fit data for third shell Sr-O interactions without the C3 term for Sr^{2+}-loaded SrMST1.

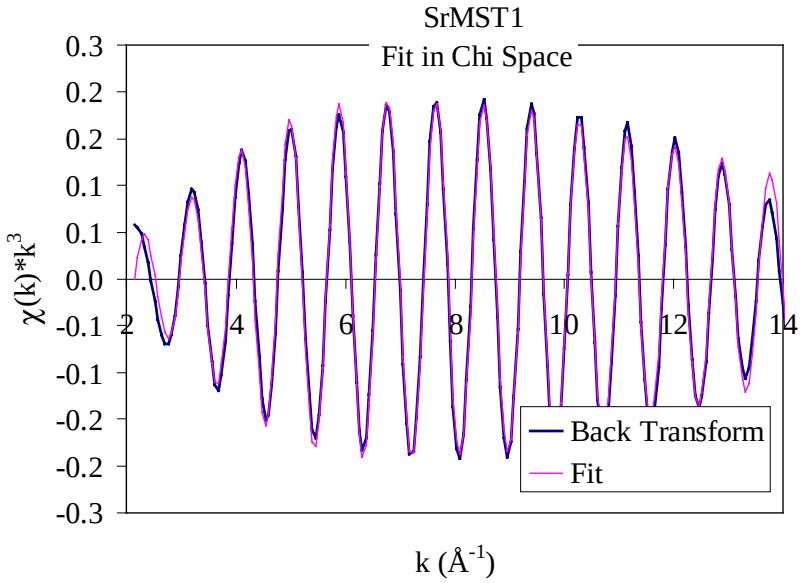

Figure 7-6 Back-transformed chi data and model fit data for third shell Sr-O interactions with the C3 term for Sr^{2+}-loaded SrMST1.

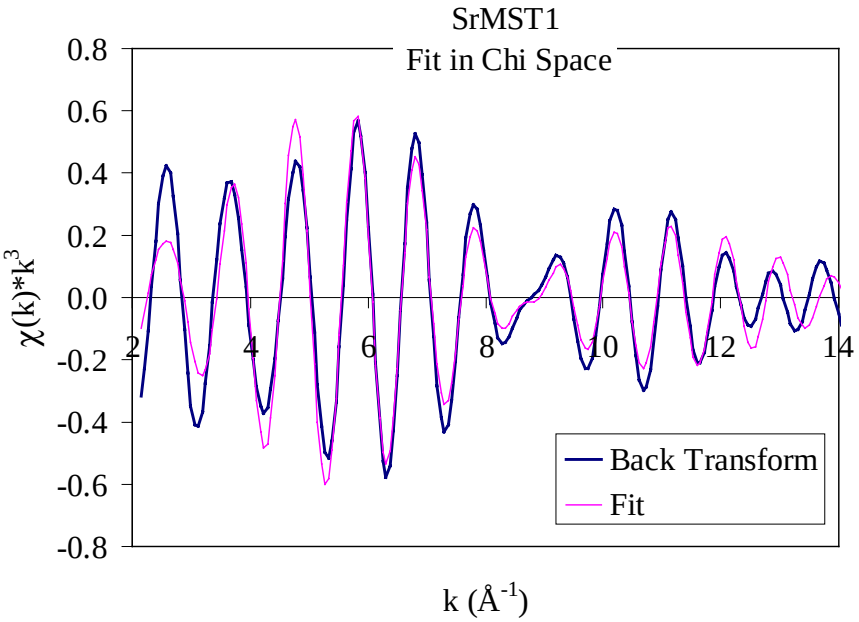

Figure 7-7 Back-transformed chi data and model fit data for interactions of second shell Sr-Ti and third shell Sr-O interactions for Sr^{2+}-loaded SrMST1—without the C3 term.

8.0 REFERENCES

[1] Stumm, W. 1992. *Chemistry of the Solid-Water Interface: Processes at the Mineral-Water and Particle-Water Interface in Natural Systems*. Wiley-Interscience, NY.

[2] McBride, M.B. 1994. *Environmental Chemistry of Soil*s. Oxford Press, NY.

[3] Sorption reversibility of sorption is tested by leaching the metal loaded solid with a target metal-free solution that has the same properties (i.e. ionic strength, background electrolytes, pH etc…) and measuring the leachate solution to determine whether any target metal is released. Specifically-adsorbed species are typically not leached with lower ionic strength solutions and specific adsorption processes are not a function ionic strength (assuming the electrolytes do not interact with the sorbed species via complexation etc.). Outer-sphere species can be readily removed with solutions of low ionic strength or solutions that contain high concentrations of a cation that has a higher affinity for the surface than the outer-sphere species. Therefore, outer-sphere sorption is viewed as reversible and a function of ionic strength whereas specific adsorption is not.

[4] Specific adsorption is typically a function of surface charge properties. When a participating surface has a charge that varies with solution pH, specific adsorption exhibits pH-dependent behavior. For example, a surface that is highly protonated (at low pH) will have more affinity for negatively-charged species (such as than negatively-charged species. As the pH decreases, the surface charge of pH-dependent charged surfaces becomes more negative and the uptake of positively-charged species is favored. Therefore, surface of metal oxides (for example) specifically adsorb more positively-charged species as the solution pH increases. However, this behavior is generalized. As the solution pH increases sorbing species undergoes a change in speciation—such as hydrolysis. In this case, the amount of specific adsorption becomes a function of solution speciation. Ion exchange resins that sorb free ions of actinides (e.g., the non-hydrolyzed Pu^{4+} species) at high H^+ concentrations (i.e., low pH) will release sorbed Pu^{4+} species when the solution pH is raised—due to the hydrolysis of the sorbed Pu^{4+} (e.g., $Pu(OH)_3^+$, $Pu(OH)_2^{2+}$). The hydrolysis species have a lower overall charge and their size (as an ion group) is larger than the free ion—making them have a lower affinity for the surface. Other processes that can influence sorption are metal complexation with ligands (i.e., with carbonate ion) or in the case of anions, protonation (e.g., $PO_4^{3-} + H^+ \rightarrow HPO_4^{2-}$). Specific adsorption processes are a function of many variables.

[5] Koningsberger, D. C. and Prins, R. 1988. *X-ray Absorption: Techniques of EXAFS, SEXAFS and XANES*, Wiley, New York.

[6] Stern, E. A. 1974. Theory of extended X-ray absorption fine structure. *Phys. Rev*. **B10**, 3027-3037.

[7] Ressler, T. (1999). *WinXAS*. A Program for X-ray Absorption Spectroscopy Data Analysis under MS Windows.

[8] Newville, M., Livins, P., Yacoby, Y., Rehr, J. J. and Stern, E. A. (1993). Near-edge X-ray-absorption fine-structure of Pb – A comparison of theory and experiment. *Phys. Rev. B-Cond. Matter*, **47**, 14126-14131.

[9] Sayers, D. E. and Bunker, B. A. (1988). In *X-ray Absorption: Techniques of EXAFS, SEXAFS and XANES*. Koningsberger, D. C. and Prins, R. (eds). Wiley, New York, Chap. 6.

[10] FEFF is a software package that was generated by researchers at the Univ. of Washington with DOE funding support. Access and use of this software is free within the DOE complex.

[11] Mustre de Leon, J., Rehr, J. J., Zabinsky, S. I. and Albers, R. C. (1991). *Ab initio* curved-wave x-ray-absorption fine structure, *Phys. Rev.* **B44**, 4146.

[12] Rehr, J. J. and Albers, R. C. (1990). Scattering-matrix formulation of curved-wave multiple-scattering theory: Application to x-ray-absorption fine structure. *Phys. Rev.* **B41**, 8139.

[13] Rehr, J. J., Mustre de Leon, J., Zabinsky, S. I. and Albers, R. C. (1991). Theoretical X-ray absorption fine structure standards. *J. Am. Chem. Soc***. 113**, 5135.

[14] Rehr, J. J., Zabinsky, S. I. and Albers, R. C. (1992). High-order multiple scattering calculations of x-ray-absorption fine structure. *Phys. Rev. Let.* **69,** 3397.

[15] Stern, E. A., Newville, M., Ravel, B., Yacoby, Y. and Haskel, D. (1995). The UWAFS analysis package - Philosophy and details. *Physica B.* **208-209**, 117-120.

[16] Axe, L., Bunker, G. B., Anderson, P. R. and Tyson, T. A. (1998). An XAFS analysis of strontium at the hydrous ferric oxide surface. *J. Coll. Interf. Sci.* **199**, 44-52.

[17] Axe, L., Tyson, T. A., Trivedi, P. and Morrison, T. (2000). Local structure analyses of strontium sorption to hydrous manganese oxide. *J. Coll. Interf. Sci.* **224**, 408-416.

[18] O'Day, P. A., Newville, M., Nuehoff, P. S., Sahai, N. and Carroll, S. A. (2000). X-ray absorption spectroscopy of strontium(II) coordination. 1. Static and thermal disorder in crystalline, hydrated and precipitated solids and in aqueous solution. *J. Coll. Interf. Sci.* **222**, 184-197.

[19] Sahai, N., Carroll, S. A., Roberts, S. and O'Day, P. A. (2000). X-ray absorption spectroscopy of strontium(II) coordination. 2. Sorption and precipitation at kaolinite, amorphous silica and goethite surfaces. *J. Coll. Interf. Sci***. 222**, 198-212.

[20] Parkman, R. H., Charnock, J. M., Livens, F. R. and Vaughn, D. J. (1998). A study of the interaction of strontium ions in aqueous solution with the surfaces of calcite and kaolinite. *Geochim. Cosmochim. Acta*. **62**, 1481-1492.

[21] In these studies, the data showing Sr and Fe (or Mn) in the second shell presents considerable confusion. Isolation of the second shell atom should provide information on whether Fe (or Mn) or Sr are present—due to the substantial difference in atomic weight. These researchers claim that they were not able distinguish Sr from a much lighter atom (Fe or Mn). Examination of the reported data indicates there may have been considerable noise, which would make distinguishing one atom from another heavier atom difficult. It is the author's opinion that this study should be redone.

[22] Pingatore, N. E., Jr., Lytle, F. W., Davies, B. M. Eastman, M. P., Eller, P. G. and Larson, E. M. (1992). Mode of incorporation of Sr^{2+} in calcite: Determination by X-ray absorption spectroscopy. *Geochim. Cosmochim. Acta***. 56**, 1531-1538.

[23] Collins, C. R., Sherman, D. M. and Ragnarsdottir, K. V. (1998). The adsorption mechanism of Sr^{2+} on the surface of goethite. *Radiochim. Acta* **77**, 201-206.

---

[24] Pfund, D. M., Darab, J. G., Fulton, J. L., and Ma, Y. (1994). An XAFS study of strontium ions and krypton in supercritical water. **98,** 13102-13107.

[25] The Sr^{2+} solutions (listed in **Table 3-2**) were selected for use as XAFS reference materials because previous XAFS studies indicated that the sorbed Sr^{2+} species remain partially hydrated upon sorption.[18,19] The Sr^{2+} solids were chosen because they could be potentially relevant phases. For example, $Sr(NO_3)_{2(s)}$ is a phase that could potentially form in NO_3-rich HLW solutions and nucleate on the MST. The Sr^{2+} in $SrTiO_{3(s)}$ may have a similar environment to that of Sr^{2+}-loaded MST solids.

[26] Teo, B. K. (1986). EXAFS: Basic Principles and Data Analysis. Inorganic Chemistry Concepts, Vol. 9, Springer-Verlag. Berlin.

[27] Cambridge Soft Corporation, 100 Cambridge Dr, Cambridge, MA.02140-2317.

[28] Behrens, E. A., Sylvester, P. and Clearfield, A. (1998). Assessment of a sodium nonatitanate and pharmacosiderite-type ion exchangers for strontium and cesium removal from doe waste simulants. *Environ. Sci. Technol.* **32**, 101-107.

[29] Hobbs, D. T., Bronikowski, M. G., Edwards, T. B. and Pulmano, R. L. (1999). Final Report on Phase III Testing of Monosodium Titanate Adsorption. WSRC-TR-99-00134, May 28, 1999.

[30] Hobbs, D. T., Blume, M. S. and Thacker, H. L. (2000). Phase V Simulant Testing of Monosodium Titanate Asdorption Kinetics, Report WSRC-TR-2000-00142.